CHARLES UNIVERSITY

Faculty of Science

Study program: Clinical and Toxicological Analysis

Bc. Anna Laštovičková

ADVANCED ELECTRON DIFFRACTION METHODS FOR STRUCTURAL DESCRIPTION OF ZEOLITES

Pokročilé metody elektronové difrakce pro strukturní popis zeolitů

Master thesis

Supervisor: Mgr. Michal Mazur, Ph.D.

Consultants: Daniel Nikolaus Rainer, Ph.D.,

doc. Maksym Opanasenko, CSc.

Prague, 2024

UNIVERZITA KARLOVA

Přírodovědecká fakulta

Studijní program: Klinická a toxikologická analýza

Bc. Anna Laštovičková

POKROČILÉ METODY ELEKTRONOVÉ DIFRAKCE PRO STRUKTURNÍ POPIS ZEOLITŮ

Advanced electron diffraction methods for structural description of zeolites

Diplomová práce

Vedoucí diplomové práce: Mgr. Michal Mazur, Ph.D.

Konzultanti: Daniel Nikolaus Rainer, Ph.D.,

doc. Maksym Opanasenko, CSc.

Praha, 2024

Prohlášení

Prohlašuji, že jsem tuto závěrečnou práci zpracovala samostatně a že jsem uvedla všechny použité informační zdroje a literaturu. Tato práce ani její podstatná část nebyla předložena k získání jiného nebo stejného akademického titulu.

Jsem si vědoma toho, že případné využití výsledků, získaných v této práci, mimo Univerzitu Karlovu je možné pouze po písemném souhlasu této univerzity.

V Praze dne 16.5.2024 Anna Laštovičková

Abstract

Electron diffraction (ED) is a powerful tool for the structure determination of crystalline materials. It offers an alternative to single crystal X-ray diffraction (SCXRD) that is often limited by the size of synthesized crystals. Electron diffraction allows analysis of materials at the nanoscale, thus it is particularly useful for samples which crystals are too small for other methods. ED utilizes electrons for collection of diffraction patterns that can be performed in a transmission electron microscope (TEM). Collected ED patterns are further analyzed allowing for the determination of unit cell parameters, lattice type, and even the crystal structure itself. Nevertheless, the effective structure determination from standard ED patterns requires in-depth expertise and data collection is time consuming. Current development of ED methods focuses on the facilitation and automatization of data collection and processing. Notably, highly advanced, continuous rotation electron diffraction (cRED) data collection takes only a few minutes enabling structure determination within a single day.

In this work, I present the utilization of cRED method for the structural characterization of zeolites. These materials are often synthesized as polycrystalline samples with crystals of nanometer in size. This makes zeolites unsuitable for structure determination using the SCXRD. Powder X-ray diffraction (PXRD) is a standard technique for the verification of zeolite structures, however, the structure determination from PXRD patterns is complex and time-consuming, e.g., due to the wide, overlapping peaks. Determination of the structure of zeolites is often essential for understanding their functionalities and potential applications. Traditionally, zeolites are synthesized through hydrothermal methods, which are non-controllable and lead to unpredictable structures. The ADOR synthesis approach offers an alternative strategy for creating new zeolite structures from parent germanosilicates. This stepwise process consists of four steps, namely: assembly of the parent material, disassembly of it into layered precursor, organization of the layers, and reassembly of them to create a daughter zeolite. This method can produce zeolites that are not possible to prepare by standard methods, however often the

quality of ADOR-prepared crystals is not suitable for their structure determination by PXRD.

The aim of this study was to utilize the cRED method to establish a unified workflow for the structure determination of novel daughter ADOR zeolites based on the analysis, mostly focused on the structure, of the parent material. To provide the control over the process optimization both parent and daughter zeolites had to be well-known and described zeolites. Thus, the most studied ADORable zeolite, UTL germanosilicate was used as a parent material. It was utilized to synthesize two daughter zeolites with recognized structures, namely IPC-2 and IPC-4. The structure, morphology, and texture of the parent UTL was investigated at first, providing valuable insights that subsequently facilitated the cRED determination of the structures of daughter materials. The successful description of investigated structures and comparison of the outcome with the literature data confirmed the validity of this method. Subsequently, it was applied to the case study of the structure determination of IPC-20, a recently published daughter zeolite prepared from IWV germanosilicate. Successful structure solution of this novel material further proved the comprehensiveness of established approach that significantly simplifies the structure determination of new ADOR zeolites.

Key words

Zeolites, germanosilicates, synthesis, ADOR approach, electron diffraction, structure determination.

Abstrakt

Elektronová difrakce (ED) je metoda používaná pro stanovení struktury krystalických materiálů. Představuje alternativu k monokrystalické rentgenové difrakci (SCXRD), která je často omezena velikostí syntetizovaných krystalů. Elektronová difrakce umožňuje analýzu materiálů v nanoměřítku, což ji činí užitečnou pro vzorky, jejichž krystaly jsou pro jiné metody příliš malé. Ke sběru difrakčních obrazců využívá elektrony a lze ji měřit v transmisním elektronovém mikroskopu (TEM). Analýzou získaných difrakčních obrazců lze stanovit parametry krystalické buňky, typ mřížky, a dokonce i samotnou krystalickou strukturu. Nicméně stanovení struktury ze standardních difraktogramů vyžaduje rozsáhlé znalosti a sběr těchto dat je časově náročný. Současný vývoj ED se zaměřuje na usnadnění a automatizaci sběru a zpracování dat. V případě kontinuální rotační elektronové difrakce (cRED) trvá sběr dat pouze několik minut, což umožňuje stanovení struktury materiálu během jediného dne.

V této práci představuji využití metody cRED pro strukturní charakterizaci zeolitů. Tyto materiály jsou často syntetizovány jako polykrystalické vzorky s nanokrystaly. Proto jejich strukturu většinou nelze určit pomocí SCXRD. Prášková rentgenová difrakce (PXRD) je standardní technikou pro ověření struktur zeolitů, avšak stanovení struktury z PXRD difraktogramů je složité a časově náročné, například kvůli širokým překrývajícím se píkům. Stanovení struktury zeolitů je klíčové pro pochopení jejich vlastností a potenciálních aplikací. Tradičně se zeolity syntetizují hydrotermálními metodami, jejichž průběh lze těžko kontrolovat a často vedou k nepředvídatelným strukturám. Alternativou je syntéza pomocí ADOR procesu, během kterého dochází k syntéze nových zeolitových struktur z mateřských germanosilikátů. Tento proces se skládá ze čtyř kroků, a to: hydrotermální syntéza mateřského materiálu, jeho rozklad (hydrolýza) na vrstevnatý prekurzor, uspořádání těchto vrstev a opětovné sestavení dceřiného materiálu. Touto metodou lze syntetizovat zeolity, které nelze připravit standardními metodami, nicméně kvalita krystalů připravených ADOR metodou je často horší, což znemožňuje stanovení jejich struktury pomocí PXRD.

Cílem této práce bylo využít metodu cRED k zavedení jednotného postupu pro stanovení struktury nových ADOR dceřiných zeolitů založeného na analýze mateřského materiálu. Pro kontrolu optimalizace tohoto postupu musely být využity známé mateřské a dceřiné zeolity. Proto byl jako mateřský materiál použit nejstudovanější zeolit pro ADOR metodu, tedy UTL germanosilikát. Tento materiál byl použit k syntéze dvou dceřiných zeolitů, IPC-2 a IPC-4. Nejprve byla zkoumána struktura, morfologie a textura mateřského UTL materiálu, což poskytlo cenné poznatky, které následně usnadnily stanovení struktur dceřiných materiálů. Úspěšné stanovení těchto struktur a porovnání výsledků s literaturou potvrdilo platnost tohoto postupu. Následně byl tento postup aplikován pro stanovení struktury IPC-20, nedávno publikovaného dceřiného zeolitu připraveného z IWV germanosilikátu. Úspěšné řešení struktury tohoto nového materiálu prokázalo komplexnost zavedeného postupu, který výrazně zjednodušuje stanovení struktur nových zeolitů syntetizovaných ADOR metodou.

Klíčová slova

Zeolity, germanosilikáty, syntéza, metoda ADOR, elektronová difrakce, určování struktury.

Acknowledgement

I would like to express my gratitude to my supervisor Mgr. Michal Mazur, Ph.D. for his support and guidance throughout my master program. Additionally, I thank my consultants, Daniel N. Rainer, Ph.D. for teaching me how to perform cRED measurements, structure determination, and data refinement, and doc. Maksym Opanasenko, CSc. for his assistance with synthesis. Furthermore, I would like to extend my thanks to Prof. Jiří Čejka and his research group (Heterogeneous Catalysis and Advanced Materials). I am especially grateful to Ing. Martin Kubů, Ph.D. for his assistance with the argon sorption measurements. Finally, I am immensely thankful for the support of my family and my partner during my studies.

Content

List of abbreviations

2D	two-dimensional
3D	three-dimensional
2D ED	two-dimensional electron diffraction
3D ED	three-dimensional electron diffraction
ADOR	assembly, disassembly, organization, and reassembly
ADF	annular dark field detector
ADT	automated diffraction tomography
BET	the method used for the calculation of surface areas based on Brunauer, Emmett, and Teller theory
CCDC	Cambridge Crystallographic Data Centre
cRED	continuous rotation electron diffraction
CTH	zeolite topology
D4R	double-four-ring
DLS	program for the simulation of crystal structures
ED	electron diffraction
EDS	energy-dispersive X-ray spectroscopy
EDT	electron diffraction tomography
IUPAC	International Union of Pure and Applied Chemistry
IPC	Institute of Physical Chemistry
IPC-1P	two-dimensional precursor obtained by hydrolysis of UTL
IPC-2	zeolite material with OKO topology
IPC-4	zeolite material with PCR topology

IPC-20	daughter material synthesized from IWV parent material
IWV	zeolite topology
IWW	zeolite topology
IZA	International Zeolite Association
OKO	zeolite topology
PCR	zeolite topology
PXRD	powder X-ray diffraction
RED	rotation electron diffraction
S4R	single-four-ring
SCXRD	single crystal X-ray diffraction
SDA	structure directing agent
SEM	scanning electron microscopy/microscope
STEM	scanning transmission electron microscopy/microscope
TEM	transmission electron microscopy/microscope
UOV	zeolite topology
UTL	zeolite topology
V_{mic}	total micropore volume
XRD	X-ray diffraction

1 Introduction

Zeolites are crystalline elementosilicates that find extensive applications in fundamental research and industry. They are widely used as catalysts, particularly in petrochemical processes like crude oil cracking.[1] Their versatility extends beyond catalysis, as they also serve as efficient ion exchangers and adsorbents.[2,3] The exploration of new applications for zeolites continues to be an active area of research, highlighting the importance of understanding and direct description of their structure.

Zeolites possess three-dimensional framework composed of TO_4 tetrahedra (where T represents a heteroatom) connected via oxygen bridges, creating a network of micropores and cavities.[4–6] The arrangement of these tetrahedra determines the zeolite's topology, leading to different framework types.[8] Traditionally, zeolites are synthesized under solvothermal conditions with the presence of structure directing agent (SDA). However, there are alternative approaches, such as ADOR, that offers alternative synthesis pathways.[6] ADOR is the abbreviation describing the four steps of this synthesis strategy consisting of: Assembly of a parent material (e.g., zeolite with UTL framework), Disassembly of the parent material into the two-dimensional precursor, which is then Organized during the third step and followed by Reassembly step of daughter material. The big advantage of this process is its controllability and predictability of the possible products of the synthesis.[6,7]

The first and the most recognized ADOR parent zeolite is UTL germanosilicate[8], which has framework consisting of dense layers connected with double four rings (D4Rs).[9] In this work, UTL zeolite was hydrothermally synthesized and subsequently used as the initial material for the synthesis of IPC-2 and IPC-4 daughter zeolites via the ADOR approach.[6] Although all three materials possess three-dimensional structures, they differ in the connecting units between their layers. The D4Rs are replaced by single-four rings (S4Rs) in the IPC-2 framework, and by oxygen bridges in IPC-4 zeolite.[6,10] This controlled variation in connectivity was achieved through various pathways of ADOR synthesis.

A variety of standard methods were utilized for characterization of these materials. These include powder X-ray diffraction (PXRD) for the description of the structure, scanning electron microscopy (SEM) for the morphology analysis, energy dispersive spectroscopy (EDS) to describe the elemental composition, and argon gas sorption for textural investigation.

The diffraction techniques were utilized for structure determination of prepared samples. Single crystal X-ray diffraction (SCXRD) would be the best technique for structure determination; however, it is rarely possible to utilize this method due to the properties of zeolite crystals. SCXRD requires single crystals of size in the micrometer range. Zeolites usually have crystals of the size in the range of nanometers, and moreover they are often polycrystalline materials. Thus, PXRD is the most commonly used method for their structure determination. Nevertheless, it is still not the perfect solution. The biggest disadvantage of PXRD is the peak overlapping which leads to time-consuming structure determination, which could take several days or even months. Therefore, electron diffraction (ED) techniques serve as another option due to its ability to study materials at the nanoscale and facilitate rapid data refinement. This often enables the determination of structure within a single day.

3D ED, specifically the continuous rotation electron diffraction (cRED) method was utilized for facile structure determination of zeolites. This method was applied first to determine the structure of UTL parent material, and then for the daughter materials. cRED measurements were performed in a transmission electron microscope (TEM). Diffraction data were collected continuously as the sample was tilted within the whole goniometer range that allows to keep the crystal in the electron beam. The acquired data allows the determination of unit cell parameters, space group, and structure itself. The entire process is depicted in Figure 1.

This work presents a workflow for structure determination of ADORable zeolites. The process began with the synthesis of a parent material, followed by the synthesis of daughter materials using the ADOR approach. The structure of the parent material was determined first. This knowledge about the parent

material's morphology, texture, and structure significantly simplified the subsequent structure determination of the daughter materials. To demonstrate the broader applicability of this workflow, it was applied to another parent material (IWV) and its daughter material (IPC-20) as a case study.

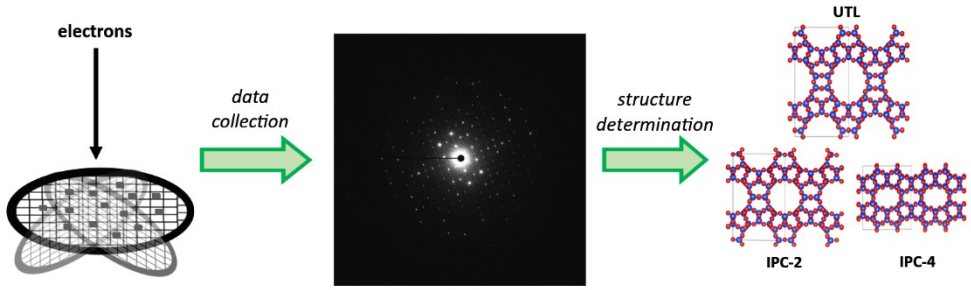

Figure 1. Scheme of a procedure for cRED diffraction data collection, processing, and structure determination.

2 Aims of the study

The aims of the master thesis were:

- Hydrothermal synthesis of parent germanosilicate (UTL) and use of ADOR approach for preparation of daughter materials, (i.e., IPC-2 and IPC-4 zeolites).
- To characterize synthesized materials by standard methods (powder X-ray diffraction, scanning electron microscopy, energy dispersive spectroscopy, and argon sorption).
- To show that insights into the properties and structure investigation of a parent zeolite used for ADOR can simplify the structure determination of daughter zeolites.
- To establish a universal workflow for structure determination of ADOR zeolites by cRED, that is based on the knowledge about the parent material.
- To apply the established workflow for the structure solution of recently synthesized novel ADOR zeolite (IPC-20).

3 Theoretical part

3.1 Zeolites

Zeolites are inorganic microporous crystalline elementosilicates containing cavities and well defined micropores. Their structures are formed by connected TO_4 tetrahedra, where T represents heteroatom such as Si, Al, Ge, Ga, or other elements.[5,6,11] These tetrahedra are connected via oxygen bridges forming three-dimensional solids. The specific arrangement of these tetrahedra determines the zeolite's topology, identified by a three-letter code assigned by the International Zeolite Association (IZA).[12,13] Zeolites can be classified based on the number of T-atoms in their pore rings as small-pore (8-rings), medium-pore (10-rings), large-pore (12-rings), and extra-large pore (bigger than 12-rings) zeolites.[11,14] This variation in pore sizes, along with differences in channel connectivity, pore geometry, and elemental composition, contributes to the diverse functionalities of zeolites.[14]

Zeolites, as so called molecular sieves, have a huge number of applications. Traditionally they are used as ion exchangers, adsorbents, and catalysts (particularly in oil refining and petrochemistry).[2,3] Nevertheless, they constantly find new applications, such as drug carriers, part of some biosensors[15], or for removal of heavy metals from the industrial wastewater[16].

Currently, over 250 zeolite topologies have been recognized by the International Zeolite Association (IZA)[13]. However, there are theoretical predictions suggesting millions of possible topologies that can be prepared, in principle.[17,18] The most common zeolites are aluminosilicates, however many of them exist as elementosilicates with boron, gallium, germanium, titanium, etc. in the structure.[19] Among these, germanosilicates have relatively open structures having extra-large pores as a consequence of the presence of secondary building units such as double four rings (D4Rs), which are rarely found in zeolites lacking germanium.[20] Germanium acts as a structure-directing agent (SDA), enabling the formation of these unique structures characterized by large pore sizes suitable for processing bulky molecules.[21]

Zeolite synthesis typically involves alkali metal ions and/or organic compounds as templates or SDAs. For high-silica zeolites, organic quaternary ammonium cations are frequently adopted as SDAs.[22] The most widely used method is hydrothermal synthesis. This synthesis involves the formation of a hydrated gel followed by a crystallization stage. A silicate or aluminum source is mixed with an SDA to create gel. This gel is then heated in an autoclave under high temperature and pressure until crystals form.[23] Solvothermal synthesis offers an alternative approach that does not involve water as a solvent (e.g., methanol or ethanol).[24] These methods allow tuning of porosity but offer limited control over the overall synthesis process itself.[6,25] In contrast, the top-down ADOR approach offers greater control over the synthesis process.[10,25]

3.2. Zeolite with UTL topology

UTL is a germanosilicate, which was reported in 2004 as the extra-large pore zeolite.[8] Its two-dimensional pore system features 12- and 14-ring channels with diameters of 8.5 × 5.5 Å and 9.5 × 7.1 Å, respectively (Figure 2). However, the presence of germanium within the framework reduces its stability, particularly in the presence of water.[9] The calcined structure degrades even under mild conditions, e.g., atmospheric moisture. This moisture sensitivity becomes an advantage in the disassembly step in the ADOR approach.[3] Notably, UTL was the first zeolite successfully transformed into individual layers, IPC-1P precursor. This precursor material features layers connected by hydrogen bonding between surface silanols.[6,9]

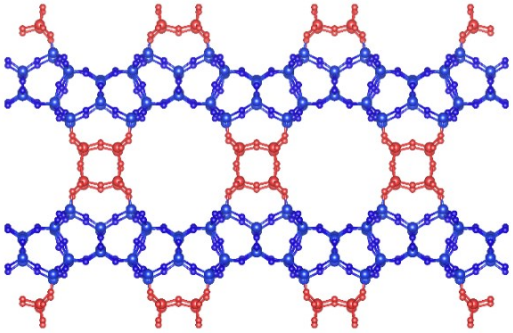

Figure 2. The structure of UTL framework. D4Rs are indicated by the red color. Silica-rich layers are depicted in blue. (adapted from IZA database[13])

3.3 ADOR

Certain structural units are selectively extracted from the parent zeolite during this process, especially those rich in hydrolytically sensitive dopant elements like germanium. After that, these units are replaced by different connecting units, forming daughter zeolites that have varied pore diameters from the parent material.[3,10] Examples of suitable parent ADOR materials include zeolites with UTL, UOV, IWW, IWV, or CTH topologies. All of them are germanosilicates containing germanium enriched D4Rs as a building unit in their structure.[7]

ADOR comprises four distinct steps. It begins with the hydrothermal synthesis of germanosilicate parent material (Assembly). The next step involves the controlled transformation of the 3D parent zeolite into a 2D layered precursor (Disassembly). This step relies on the selective hydrolysis of the germanium-oxygen bonds within the germanium-rich D4Rs, leaving the bonds within the silica layers intact. Following disassembly, the obtained 2D layered precursor is organized. Various techniques can be employed for this purpose, including the intercalation of an organic agent, direct calcination to condense the layers, or the introduction of additional silica sources. The final step involves the reconnection of the layers (Reassembly). This is achieved by heating the sample at temperatures exceeding 500 °C, a process also referred to as calcination.[6,7] The entire ADOR process is schematically illustrated in Figure 3.

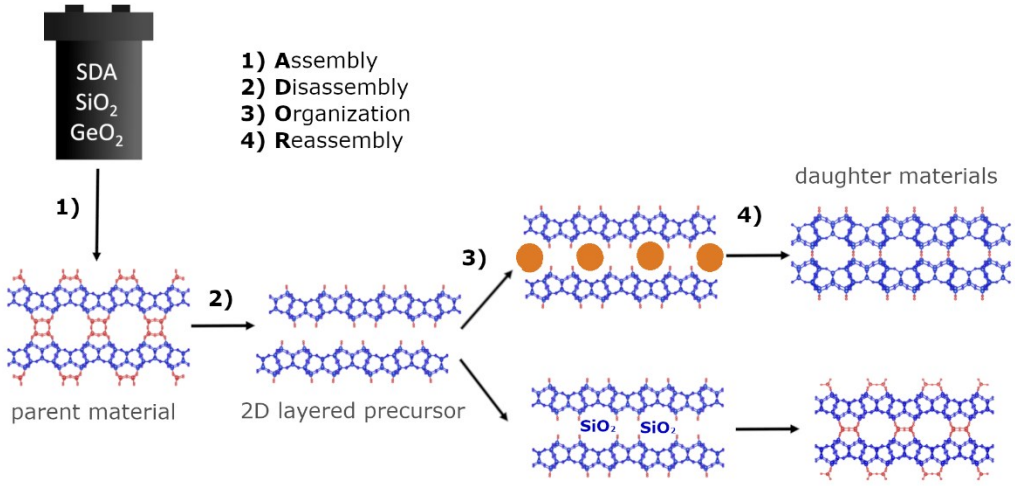

Figure 3. Scheme of ADOR approach. Reaction mixture in a stainless steel autoclave used for assembly of parent zeolite (1); disassembly into 2D precursor (2); organization, the orange dots represent organic molecules used for organization of layers, second type of connecting units that organize layers can be produced by intercalation of additional silica (3); reassembly step of the process produces 3D daughter zeolites (4).

3.4 Zeolite with OKO topology

IPC-2, a daughter material of UTL, possesses the OKO topology[10] as illustrated in Figure 4. This medium/large pore zeolite features a combination of 10- and 12-ring channels, offering a different pore structure compared to its parent UTL. It contains single-four-rings (S4Rs) as connecting units between UTL-like layers. IPC-2 can be synthesized in two different ways. The first, known as the inverse sigma transformation route, involves hydrolyzing the daughter material under highly acidic conditions using a HCl solution. Contact with ambient air is minimized during this process. Alternatively, the second option employs post-synthetic intercalation of silica species into the IPC-1P layered precursor. This way is also called the stabilization process.[3,25]

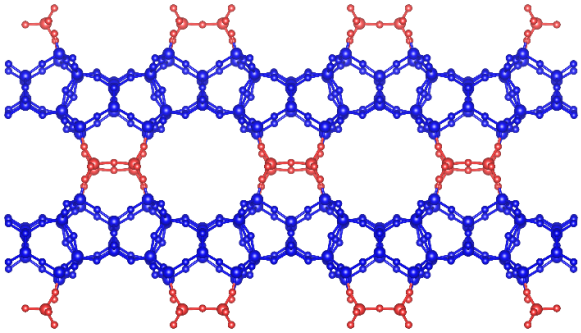

Figure 4. The structure of OKO framework. S4Rs are in the red color. Silica-rich layers are depicted in blue. (adapted from IZA database[13])

3.5 Zeolite with PCR topology

IPC-4, another daughter material derived from UTL, has PCR topology[10], which is shown in Figure 5. This material exhibits a small/medium pore structure with rings composed of 8- and 10-tetrahedral units. Unlike IPC-2, IPC-4 does not contain S4Rs, but has oxygen bridges as connecting units.[25] The synthesis of IPC-4 involves the condensation of IPC-1P layers. A crucial step in this process is the organization of these layers using an organic molecule, e.g., octylamine. This organic molecule is subsequently removed through calcination.[10,25]

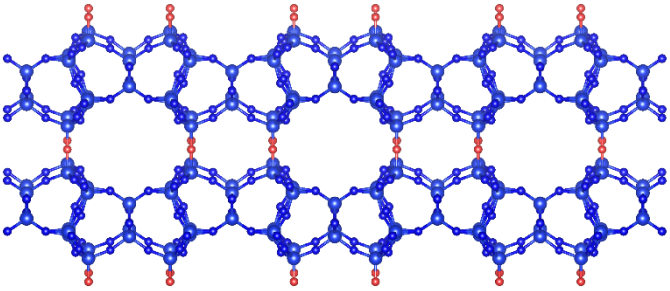

Figure 5. Structure of PCR framework. Oxygen bridges are marked with red color. Silica-rich layers are depicted in blue. (adapted from IZA database[13])

3.6 Structural characterization

Diffraction is a phenomenon, which occurs in crystalline materials. It is a form of elastic scattering, characterized by a wave encountering an obstacle and bending around it, subsequently spreading out in a new direction.[26] Diffraction

techniques utilize radiation sources like X-rays, electrons, or neutrons, which all operate on the same fundamental principle. X-ray diffraction can be used for thin samples as well as for bulk materials, while electron diffraction is utilized only for thin samples due to the short penetration depth of electrons.[27] Neutron diffraction is complementary to X-ray and electron diffraction. Neutrons interact with nuclei and can provide information about magnetic structure, or the position of light elements like hydrogen. Nevertheless, neutron sources are more expensive, thus much more commonly used standard technique is X-ray diffraction.[28,29] In this thesis, X-ray and electron diffraction were utilized and discussed.

3.6.1 X-ray diffraction (XRD)

X-ray diffraction (XRD) stands as a universal and non-destructive technique for characterizing a wide range of crystalline materials, including minerals, metals, polymers, ceramics, and plastics. It utilizes X-rays, electromagnetic waves with short wavelengths ranging from 0.01 nm to 10 nm, corresponding to energies spanning from 0.125 keV to 125 keV. XRD offers the versatility to analyze both single crystals (SCXRD) and powdered samples (PXRD).[30,31]

A diffraction pattern is the outcome of an XRD measurement. This pattern comprises peaks with varying intensities and positions. The investigation of the pattern can provide information concerning atom arrangement, the position of atoms, and the atomic spacing angles.[30,31] Thus, XRD emerges as an indispensable tool for unraveling the structure of zeolites and other crystalline materials.

According to Bragg's theory, crystals possess lattice planes with specific spacing distance *d*. When X-rays interact with atoms in these atomic planes, they generate reflected beams. This relationship is described by Bragg's law:

$$n\lambda = 2dsin\theta, \qquad (1)$$

where λ is X-ray wavelength, n order of reflection, d spacing distance and θ angle of diffraction beam.[31]

Single crystal X-ray diffraction (SCXRD) is the most used method for determining crystal structures. However, it requires large, high-quality single crystals, at least of a few micrometers in size.[32] During the measurement, the mounted crystal is rotated around, for example using a four-circle goniometer. Rotations of crystals at the four angles allows the collection of data that contain the information about the relationship between the crystal lattice, source X-ray beam, and detector.[30,33] The main limitations of this technique are the requirement of large crystals[34], which can be challenging to obtain for certain materials like zeolites, and the potential presence of defects or disorders within the crystals, which can make the analysis unfeasible.[33]

Powder X-ray diffraction (PXRD) is a powerful technique for characterizing the structure of powdered materials. It is particularly useful for samples with crystals too small for SCXRD analysis, typically in the nanometer range.[33] PXRD provides valuable information such as phase identification, sample purity, and crystallite size.[35] However, determining the structure of unknown material from PXRD data can be challenging due to the peak overlap.[36,37] Millions of randomly oriented crystals contribute to the diffraction pattern, resulting in diffraction rings instead of points. Additionally, compressing the 3D reciprocal space into a 1D pattern can lead to overlapping reflections. This overlap becomes more pronounced with the larger unit cells.[33]

Several techniques exist to refine crystal structures, including the Rietveld method for quantitative phase analysis of PXRD data.[38] This method compares the measured diffractogram with calculated patterns, refining instrumental and structural parameters until the best fit is achieved. This allows the refinement of structure parameters such as atomic positions, occupation factors, and atomic replacement within a material.[30] Le Bail fitting is a structureless fitting method used to extract reflection intensities from PXRD data, providing accurate unit cell parameters in a much faster process compared to Rietveld refinements.[39]

Zeolites are often polycrystalline materials, presenting unique challenges for structure determination using XRD.[36] Their small crystal size, large unit

cells, and inherent disorder can lead to closely spaced peaks in the diffraction pattern.[37] This peak overlap can introduce errors during structure determination, particularly for materials with large unit cells.[40]

3.6.2 Electron diffraction (ED)

Although X-ray diffraction techniques like SCXRD and PXRD are powerful tools for structure determination, they have some limitations. Electrons offer an alternative. They interact with matter roughly 10^6 times more strongly than X-rays, making them ideal for analyzing crystals that are too small for SCXRD or too complex for PXRD.[40,41] However, these strong interactions come with drawbacks. Electron beams can damage samples and can undergo multiple scattering. This means they are diffracted more than once when passing through a material. Consequently, the resulting diffractions exhibit a dynamical effect, where the intensities are not directly related to the structure factors.[33,42]

Despite these challenges, 3D electron diffraction (3D ED) has emerged as a powerful technique for structure determination. It collects data in the three-dimensional reciprocal space using various methods like automated diffraction tomography (ADT), rotation electron diffraction (RED), electron diffraction tomography (EDT), and continuous rotation electron diffraction (cRED).[43] Notably, 3D ED data can be treated similarly to SCXRD data, allowing for the use of familiar processing programs.[44]

The resulting diffraction pattern reveals information about the crystal structure. The positions of the diffraction spots define the unit cell parameters, and lattice type. The spot intensities are related to the atomic positions, while the overall pattern reflects the crystal's symmetry.[44]

This technique has proven particularly valuable for the characterization of zeolites. Several of them have been solved using 3D ED. It makes this method highly valuable because more than millions of potential zeolite structures were theoretically predicted, thus fast and precise structural investigation supports the verification of synthesis efforts.[42]

3.6.2.1 Continuous rotation electron diffraction (cRED)

Within 3D ED, continuous rotation electron diffraction (cRED) stands out as a powerful tool for analyzing nanocrystals. In cRED, diffraction patterns are collected continuously as the sample rotates within the whole goniometer range, which makes the measurement fast.[44,45]

While limitations like multiple scattering persist, cRED offers advantages. The dynamical effect is reduced compared to 2D ED due to the off-axis crystal orientation during measurement.[39,45] This allows treating diffraction spot intensities as kinematical intensities, enabling the use of SCXRD software for data processing. Additionally, continuous data collection overcomes the problem with beam damage, because data are collected in a short time.[32]

The experimental simplicity of cRED is another advantage. Data collection can be completed within a few minutes[46], the goniometer tilting to acquire a 3D diffraction set. The data collection is controlled only by software, which makes it possible to measure by conventional transmission electron microscope (TEM). The collected patterns are merged to construct a 3D reciprocal lattice. These data are then used to determine unit cell parameters and crystal structure.[40,44]

3.7 Standard characterization techniques

3.7.1 Scanning electron microscopy (SEM)

A scanning electron microscope (SEM) utilizes a focused beam of electrons to investigate a sample's surface topography and morphology. Electrons, generated by an electron gun, are accelerated by positive electrical potential, and shaped into a focused beam using electromagnetic lenses. The electron energies are typically in the range from 1 to 30 keV.[47] This beam interacts with the sample within a vacuum chamber, which is crucial to prevent interactions with air molecules that could degrade the beam intensity and stability. The interaction between electrons and the sample generates various signals. Detectors collect

secondary electrons (low kinetic energy) or backscattered electrons (high kinetic energy), revealing information about the sample surface.[48–50]

A significant advantage of SEM lies in its relatively simple and rapid sample preparation. Unlike transmission electron microscopy (TEM), samples do not require to be electron transparent.[50]

3.7.2 Transmission electron microscopy (TEM)

Transmission electron microscopy (TEM) offers high-resolution imaging of sample structure. Unlike SEM, TEM utilizes a focused beam of high-energy electrons (typically 80 to 300 keV) that can penetrate samples with less than 100 nm thickness.[47,50,51]

The microscope contains a series of electromagnetic lenses. Condenser lenses focus the electrons into a beam, objective lenses focus the transmitted electrons to form an image, and projector lenses magnify the image onto a detector. Additional lenses can be used to scan the beam across the sample, creating a scanning (STEM) mode.[47,51,52]

TEM offers two imaging modes: bright-field and dark-field. In bright-field, only transmitted electrons reach the detector. On the other hand, dark-field mode blocks transmitted electrons with an aperture, allowing only diffracted electrons pass through.[53]

3.7.3 Energy dispersive X-ray spectroscopy (EDS)

Energy dispersive X-ray spectroscopy (EDS) is a powerful technique often used in conjunction with SEM or STEM. It provides information about the approximate elemental composition of a sample. This technique is capable of detecting nearly all elements except those, which do not emit X-rays.[38,49]

EDS works by analyzing the X-rays emitted by the sample when bombarded with a focused electron beam.[49] These electrons, with energies up to 300 keV, interact with atoms within the sample. The interaction results in the ejection of secondary electrons from the inner shell of the atoms. Subsequently, an electron from an outer shell fills the vacancy, leading to the emission of an

X-ray photon with a specific energy determined by the difference in binding energies between the shells.[54] EDS detectors capture these characteristic X-rays. By analyzing the X-ray spectrum, EDS can identify the elements present within the sample. The intensity of detected radiation is directly proportional to the quantity of the element in the sample.[55]

3.7.4 Argon sorption

Gas adsorption is a powerful tool for characterizing porous materials. Unlike chemisorption, which involves chemical bonds, gas adsorption relies on weak van der Waals forces to attract gas molecules (adsorbates) to the surface of a material (adsorbent).[56] This technique is widely used to determine various properties of porous materials, including surface area, pore size distribution, and total pore volume.[56,57] Small molecules like argon and nitrogen are commonly used as probe molecules in gas adsorption. Argon is particularly useful for analyzing micropores.[58] The amount of adsorbed gas is determined by either a change in pressure (volumetric method) or the increase in mass of the sample (gravimetric method).[59]

The gas adsorption process begins with gas molecules accumulating on the material's surface at low pressures. As the pressure increases, more gas is adsorbed on the surface. Further pressure increases lead to the formation of the multilayer. The smaller pores fill up first, followed by larger ones. Eventually, at high pressures, all pores become filled with gas molecules. By tracking the desorption of gas, it is possible to reveal the shape of pores, e.g., by description of the type of hysteresis loop.[60] Hysteresis loop gives information on the mechanism of adsorption and desorption in mesopores, which allows the assumption of pore geometry. There are six different types of hysteresis loops, each associated with different types of porous structures.[61]

IUPAC classifies gas adsorption isotherms into eight distinct types. Type I isotherms are characteristic for microporous materials like zeolites. These can be further classified into type I(a) for materials with pore size below 1 nm and type I(b) characterized by monolayer adsorption. Type II isotherms indicate nonporous or microporous materials with significant multilayer adsorption.

Type III and V isotherms suggest weak interaction between the adsorbate and the adsorbent in nonporous or microporous materials. Type IV is also divided into two types: type IV(a) with a hysteresis loop for materials with pore width greater than 4 nm, and type IV(b) without a hysteresis loop for materials with pore width smaller than 4 nm.[62] Type VI isotherms represent highly uniform nonporous surfaces.[59,63]

4 Experimental part

4.1 List of chemicals

Table 1. List of chemicals used for the synthesis of structure directing agent, UTL, IPC-1P, IPC-2, and IPC-4.

Chemical	Purity	Manufacturer
1,4-dibrombutane	99%	Sigma Aldrich
2,6-dimethylpiperidine	≥ 99%	TCl Chemicals
1-octylamine	99%	Alfa Aesar
Acetic acid	99%	Lachner
Acetonitrile	≥ 99%	Sigma Aldrich
Ambersep 900 resin	–	Sigma Aldrich
Cab-O-Sil M-5	–	Acros Organic
Diethylether	–	VWR Chemicals
Ethanol	99.80%	VWR Chemicals
Germanium dioxide	≥ 99.99%	Sigma Aldrich
Hydrochloric acid	37%	VWR Chemicals
Potassium carbonate anhydrous	p.a.	Lachner

4.2 Synthesis of zeolites using ADOR approach

4.2.1 Synthesis of structure directing agent

2,6-dimethyl-5-azoniaspiro[4.5]decane bromide was selected as the SDA for UTL synthesis.[64] In a first step, 30 ml of 1,4-dibrombutane, 41.5 g of K_2CO_3, and 640 ml of acetonitrile were mixed. Subsequently, 35 ml of 2,6-dimethylpiperidine was slowly added dropwise to the reaction mixture under continuous stirring. The mixture was then heated under reflux at 85°C overnight. The next day, the solvent was removed using a vacuum rotary evaporator. Excess of ethanol (approximately 400 ml) was added to the residual solid. The mixture was then filtered to remove K_2CO_3. The filtrate was concentrated by evaporating

the solvent until a saturated solution was obtained. White solid product was precipitated by addition of diethyl ether. The solution was filtered again, and the solid product was washed with diethyl ether. Finally, the sample was dried overnight under ambient air conditions. The successful synthesis of SDA was confirmed by ^{1}H NMR spectroscopy using deuterated chloroform as the solvent.

4.2.2 Synthesis of UTL

The synthesis gel was prepared in the ratio 1 SiO_2 : 0.5 GeO_2 : 0.5 SDA : 35 H_2O. Prior to gel preparation, the synthesized SDA underwent ion exchange. Ambersep 900 resin in hydroxide form was first washed with distilled water. Then, 39.4 g of the SDA was dissolved in 200 ml of distilled water, and the washed resin was added. The mixture was stirred for 3.5 hours. The resin was subsequently removed by filtration. To the filtered solution, 19.1 g of silica source (Cab-O-Sil M5) and 16.6 g of GeO_2 were added. The mixture was stirred again for 40 minutes. The resulting gel had a final pH of 11. The prepared gel was transferred into 100ml autoclaves and placed in a rotatory oven for the synthesis. The reaction conditions were set at 175 °C for 10 days. After the reaction period, the autoclaves were cooled down. The solid product was separated by filtration and washed distilled water until the pH reached 7. The final product was then dried in an oven at 60 °C overnight. The dried material was calcined to remove organic template and to achieve the final zeolite structure. This calcination was performed in air at 550 °C for 6 hours with a temperature rate of 1 °C per minute.[65]

4.2.3 Synthesis of IPC-1P

The calcined UTL was mixed with 1M CH_3COOH in 1 g:200 ml ratio (UTL:CH_3COOH). The mixture was then refluxed at 75 °C overnight. Afterwards, the solid product was separated by filtration and washed with distilled water. The final product was dried in an oven at 60 °C overnight.[3]

4.2.4 Synthesis of IPC-2

IPC-2 was synthesized using the inverse sigma transformation route.[3] Calcined UTL was subjected to hydrolysis using a strong acid solution. The UTL was

mixed with 12M HCl in 1 g:160 ml ratio (UTL:HCl). The mixture was then refluxed at 100 °C for 24 hours. Following hydrolysis, the solid product was filtered and washed with distilled water to reach pH 7. The sample was dried in an oven at 60 °C overnight. The dried material underwent a calcination, which was performed in air at 550 °C for 6 hours with temperature rate of 1 °C per minute.

4.2.5 Synthesis of IPC-4

IPC-4 was synthesized using an intercalation of an organic molecule.[10] 0.37 g of IPC-1P was mixed with 31.6 ml of 1-octylamine. The mixture was then refluxed at 70 °C for 7 hours. After refluxing, the mixture was stirred overnight at room temperature without additional heating. The following day, the solid product was separated by centrifugation and washed with distilled water. The material was then dried in an oven at 60 °C. The final step involved calcination, which was performed in air at 550 °C for 6 hours with temperature rate of 1 °C per minute.

4.3 Characterization methods

4.3.1 PXRD

The structure and crystallinity of prepared samples were investigated by powder X-ray diffraction. Bruker AXS D8 Advance powder diffractometer equipped with a LYNXEYE-XE detector using Cu Kα radiation in Bragg-Brentano geometry was used. All obtained data were compared with literature and IZA database[13]. Le Bail fitting of PXRD patterns was performed in Jana2020[66].

4.3.2 SEM

The morphology of prepared samples was examined by SEM using a JEOL IT-800 scanning electron microscope (Viničná Microscopy Core Facility, VMCF of the Faculty of Science, Charles University) equipped with field-emission gun operating at 1 kV. The secondary electrons were used for imaging in the charge-free mode.

4.3.3 STEM-EDS

STEM-EDS was utilized for imaging and elemental mapping of prepared materials. Measurements were performed on JEOL JEM NEOARM-200F microscope equipped with Schottky-type field emission gun operating at 200 keV. The sample was deposited on the carbon coated copper grid. Images were collected with an annular dark field (ADF) detector.

Elemental analysis was performed in-situ in the STEM microscope using JEOL JED-2300 EDS spectrometer. Due to the beam instability of the sample EDS maps were collected for over 20 minutes to provide sufficient signal to noise ratio and simultaneously with a dead time of 2 % to avoid the damage of the samples by the electron beam.

4.3.4 Argon sorption

The textural properties of all samples were measured on Micromeritics 3Flex volumetric Surface Area Analyzer (Version 5.02). Argon was used as adsorptive for the adsorption/desorption measurements. Prior to measurement, all samples were degassed by heating at 250 °C for 8 hours using Micrometrics Smart Vac Prep instrument. BET areas were determined from adsorption data in the p/p^0 range of relative pressure from $p/p^0 = 0.01$ to $p/p^0 = 0.20$. The total micropore volume was obtained by t-plot method. All measurements were performed at −186.15 °C (87 K).

4.4 cRED

JEOL JEM NEOARM-200F was used for electron diffraction measurements. A carbon coated copper grid served as the substrate for all measurements. Wet sample preparation was employed. To achieve a homogeneous distribution, 1 mg of the sample was ground to break up agglomerates and generate smaller particles. The ground sample was then dissolved in ethanol to create a suspension. This suspension was sonicated for several minutes to further disperse the particles. Subsequently, a single droplet of the suspension was deposited onto the prepared grid. Following solvent evaporation at room temperature, the grid was loaded onto the high-tilt tomography TEM holder

(Figure 6). The holder was then inserted into the transmission electron microscope.

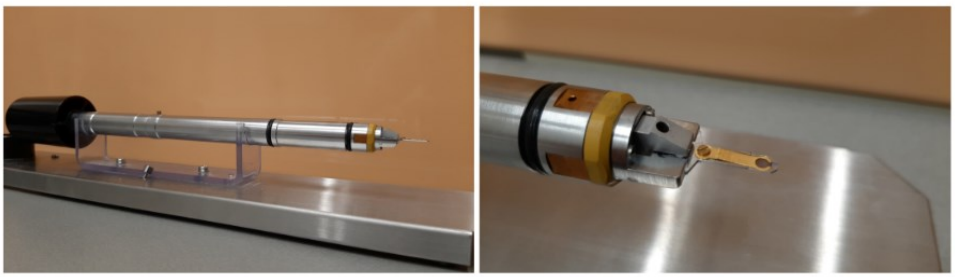

Figure 6. High-tilt tomography TEM holder with loaded grid.

The initial step in 3D ED involved microscope alignment, which consists of gun alignment, condenser and objective lenses alignment, and correction of the astigmatism. Afterwards, a suitable single crystal must be found for the measurement. This crystal should be single without any other phases or intergrowths, thin, not surrounded by other crystals, and not at the edge of the grid.

Python software instamatic[67] version 1.7.0 together with EMMenu 5.0.21.0 program was used for the data collection. For measuring a crystal, Z height was adjusted to minimize crystal movement during the measurement. The holder was tilted within a whole goniometer range and data were collected continuously, typically from –70 ° to +70 °, however the maximum tilt depended on the location of the crystal on the grid (e.g., the range of a tilt for crystals located closer to the edge of copper grid was limited).

4.5 Structure determination and refinement

The collected ED data were processed using python script TVIPS from instamatic. First, the program REDp[68] was used for reconstructing the 3D reciprocal lattice and its investigation. A beam-stop mask was added, and a conventional peak search was performed. The found peaks were then merged. These merged peaks served as the basis for determining the initial unit cell parameters. Finally, the REDp program facilitated the analysis of 2D slices

extracted from the 3D reciprocal lattice data. This analysis enabled the identification of possible space groups for the crystal.

Following the initial processing using REDp, the program XDS[69] was utilized to determine the unit cell parameters. Notably, while XDS was originally developed for SCXRD, its capabilities can be employed for ED data analysis as well. XDS processed the diffraction patterns and generated a .hkl file. A .ins file was created by python script edtools. Both these files were used by SHELXT[70,71] program to solve the crystal structure. Finally, the obtained structure solution was refined using SHELXL[70] in the OLEX2 program. This refinement process led to the generation of the final .cif file with a structure solution.

The completeness of a dataset is dependent on the tilt range during data collection. Higher symmetry systems usually achieve better data completeness. Although structures can potentially be solved from datasets with completeness around 50 %, merging multiple datasets is a common strategy to achieve a higher overall completeness, improving the quality of the final structural model.[72]

Each data set and structure are accompanied by an R-factor. The R-factor is a metric used to estimate the quality of a structure solution, with lower values indicating a better fit between the observed and calculated diffraction data. It can be calculated by this formula:

$$R = \sum|F_o - F_c| / \sum|F_o|, \quad (2)$$

where F_o is observed structure factor and F_c is calculated structure factor of a given reflection.[73]

This R-value is also called R_1 factor. An ideal structure solution would have R-values of 0 but this is never achieved in practice. The R_w factor is similar to the R1 factor but refers to squared F-values. The value of R_w is usually higher than R_1.[74]

5 Results and discussion

This work aimed at the establishment of the workflow for the facile structure solution of ADOR zeolites. The material chosen for the preparation of the workflow was the first, and most investigated parent ADOR zeolite, UTL. It was prepared by hydrothermal synthesis and transformed into two daughter zeolites by the ADOR approach. The synthesis provided three materials that were characterized by standard techniques that allowed to confirm the successful synthesis. Moreover, this basic analysis allowed the comparison between parent and daughter material's properties, such as the crystal morphology, as an initial input for more sophisticated structural analysis, and eventually, the full structure determination. The location of germanium within the structures was not determined in this study.

5.1 Standard characterization techniques

The basic characterization of synthesized samples is based on the verification of their structure, texture, morphology, and elemental composition.

A standard control of the crystallinity of synthesized material is usually performed by PXRD. The experimental PXRD pattern of UTL parent material was compared to the theoretical one, which can be found in the IZA database[13] (Figure 7). This comparison confirmed that the synthesized material possesses the UTL framework topology. Among the others, the presence of a characteristic interlayer peak at 6.1° served as a strong confirmation of UTL framework structure. Based on Bragg's law, this peak position corresponds to a d-spacing between the layers of approximately 1.45 nm.

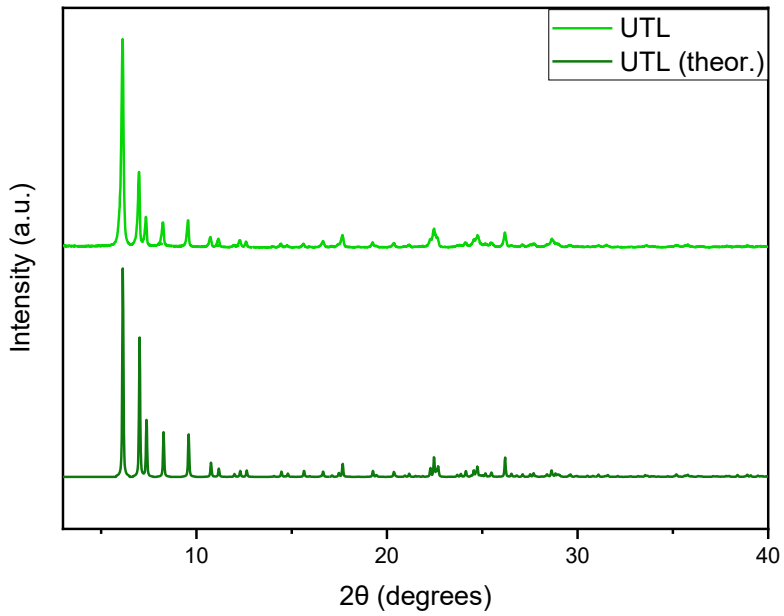

Figure 7. PXRD patterns of UTL. Synthesized material (light green) and theoretical PXRD pattern of UTL adapted from IZA database[13] (dark green).

Figure 8 presents the PXRD patterns of the prepared daughter materials compared with the parent one. PXRD analysis confirmed that IPC-2 and IPC-4 were successfully synthesized as daughter materials from the parent UTL zeolite using the ADOR approach. As mentioned before, the transformation of UTL into other structures can be tracked by the analysis of the PXRD patterns. The most indicative feature allowing to track the successful ADOR is the position of the interlayer peak, represented by (200) reflection in PXRD pattern. Both daughter materials exhibit a shift of the interlayer peak towards higher angles compared to UTL. This shift indicates a decrease in the d-spacing between the layers. The interlayer peak positions are observed at 7.7 ° and 9.6 ° for IPC-2 and IPC-4, respectively. Applying Bragg's law, these interlayer peak positions correspond to d-spacing of approximately 1.15 nm for IPC-2 and 0.92 nm for IPC-4. This observed decrease in the d-spacing is attributed to the introduction of different connecting units within the framework during the ADOR process.

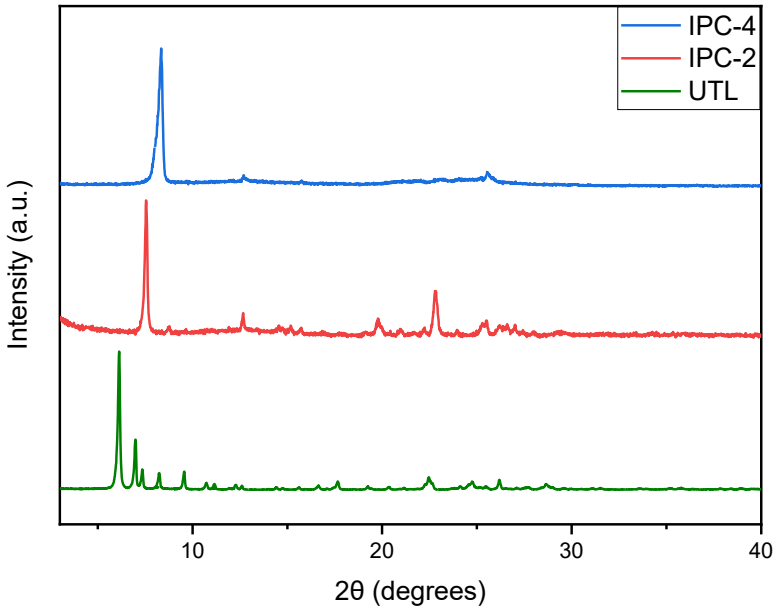

Figure 8. Measured PXRD patterns of UTL (green), IPC-2 (red) and IPC-4 (blue).

Argon sorption measurements were used to investigate the textural properties of synthesized materials. All three isotherms, presented in Figure 9, exhibit a type I(a) isotherm, typical for microporous materials. Moreover, the isotherm for IPC-2 has a hysteresis loop at higher pressures, indicating the presence of mesopores. This mesoporosity most likely originates from interparticle adsorption caused by the presence of polycrystals, which can be observed in SEM images (see Figure 10 presented below).

The analysis revealed significant differences in total micropore volume between the samples. UTL exhibited the highest total micropore volume (0.21 $cm^3 \cdot g^{-1}$), corresponding to its large pore system. Conversely, IPC-4 showed the lowest micropore volume (0.07 $cm^3 \cdot g^{-1}$), which corresponds with the decrease in pore size. The Brunauer-Emmett-Teller (BET) model was used to calculate the total surface area for each material. UTL possessed the highest surface area (507 $m^2 \cdot g^{-1}$), followed by IPC-2 (416 $m^2 \cdot g^{-1}$) and IPC-4 (225 $m^2 \cdot g^{-1}$). This trend correlates with the size of the channel system, where UTL has the largest channels. All measured parameters are summarized in Table 2.

Table 2. Textural properties of synthesized materials. BET areas (BET) and total micropore volume (V_{mic}).

sample	BET [$m^2 \cdot g^{-1}$]	V_{mic} [$cm^3 \cdot g^{-1}$]
UTL	507	0.21
IPC-2	416	0.16
IPC-4	225	0.07

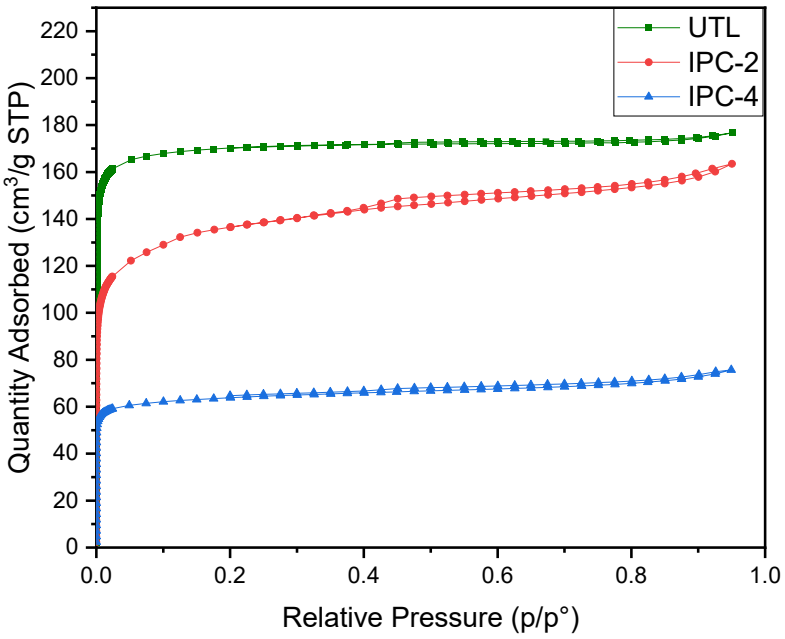

Figure 9. Argon isotherms of parent material of UTL (green), and synthesized daughter materials IPC-2 (red) and IPC-4 (blue).

SEM was used to investigate the morphology of crystals. As shown in Figure 10, the images reveal plate-like crystals stacked upon each other. This similar morphology observed across all samples suggests that the crystal morphology of the parent UTL material was preserved during the ADOR process and remained unchanged in the daughter materials. The presence of polycrystalline aggregates in all samples precludes measurement by SCXRD. However, the information obtained from the SEM images regarding crystal habit facilitated subsequent TEM and, most importantly ED measurements.

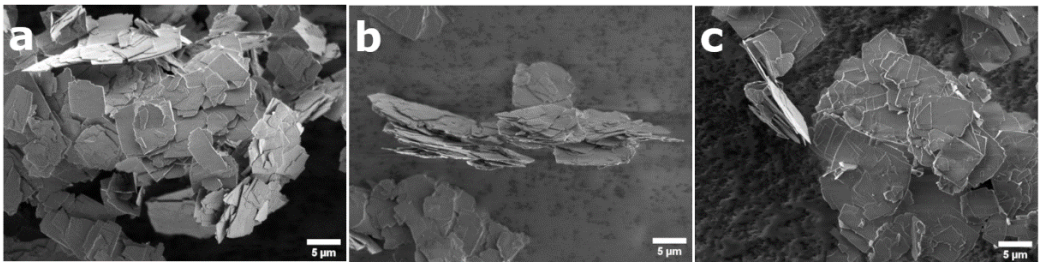

Figure 10. SEM images of UTL (a), IPC-2 (b) and IPC-4 (c).

Similar to the SEM, STEM imaging (Figure 11) revealed plate-like crystals stacked upon each other. STEM-EDS analysis provided valuable insights into the elemental composition of prepared materials. The parent material contains the highest germanium content with a silicon/germanium ratio of 4.2. This aligns well with the reported values for UTL material. Most of the germanium is removed during the hydrolysis step in the ADOR approach, explaining the significant decrease observed in daughter materials, IPC-2 and IPC-4. Both daughter materials showed very low germanium content. The analysis also confirmed a uniform distribution of silicon and germanium within all samples.

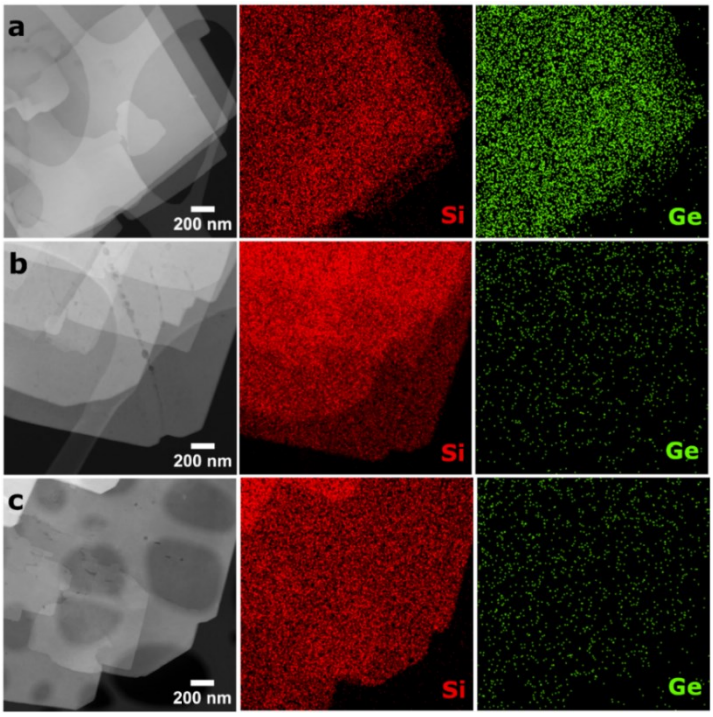

Figure 11. STEM-EDS micrographs with corresponding EDS maps for silicon (red) and germanium (green) of UTL (a), IPC-2 (b) and IPC-4 (c).

Comprehensive characterization of the parent material using standard methods established its crystallinity, crystal morphology, textural properties, and elemental composition. The subsequent application of these same techniques to the daughter materials revealed significant structural similarities, facilitating their structure determination, which is shown in the following chapters.

5.2 Structure determination of parent material

The measured PXRD pattern was fitted using the Le Bail method implemented in the Jana2020 program using published unit cell parameters for the UTL framework as starting values[13]. The resulting fit is presented in Figure 12. The obtained cell parameters in the fixed monoclinic unit cell with *C*2/m space group are as expected for UTL (see Table 3). The quality of the fit is indicated by the R_w value of 0.1502.

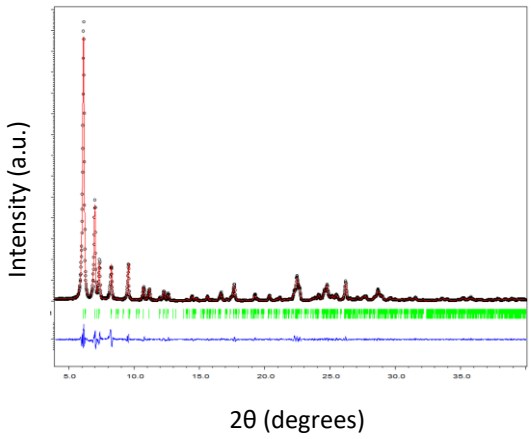

Figure 12. Le Bail fit of PXRD pattern of UTL.

The initial structure determination of the parent material employed cRED. A total of 491 frames were collected across a 129.67° rotation angle, starting at −64.27 ° and ending at +65.40 ° with a speed of 0.661 degrees per second. Investigation of merged ED patterns using REDp software revealed a C-centered monoclinic Bravais lattice, corresponding to the 2/m Laue class. The reflection conditions, essential for space group determination, were analyzed from the individual slices presented in Figure 13. The conditions are $h + k$ for (hk0), h for (h0l), and k for (0kl). Based on these conditions and literature[75], the

possible space groups for the parent material were identified as *C*2 (number 5), *C*m (number 8), or *C*2/m (number 12).

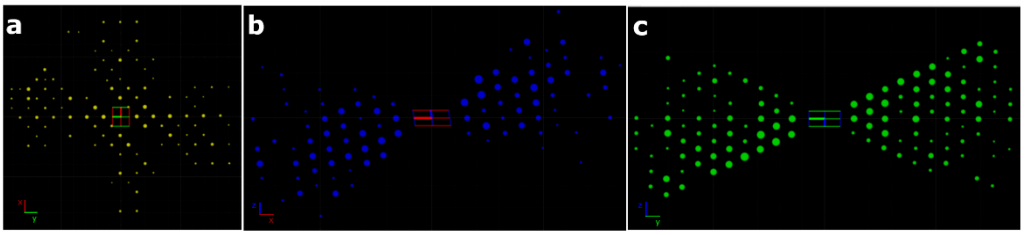

Figure 13. 2D slices of the reciprocal lattice of UTL derived from the 3D cRED data. 2D (hk0) slice (a), 2D (h0l) slice (b), and 2D (0kl) slice (c).

The XDS program was subsequently used for data reduction and integration. These calculations confirmed the monoclinic C-centered (m*C*) Bravais lattice with the following cell parameters: a = 30.240 Å, b = 14.312 Å, c = 12.569 Å, α = 90.000 °, β = 105.318 °, γ = 90.000 °. During the integration step, the common space group in the lowest symmetry (*C*m, number 5) was chosen based on the reflection conditions previously determined. The data obtained in this process had a completeness of 82.9 %, and observed R factor was 10.1 %.

Table 3 compares the unit cell parameters obtained from the XDS program with those derived from Le Bail method and theoretical values from the IZA database. Discrepancies are observed between these values due to the several factors. The IZA database values were obtained from a DLS-refinement[76] in the highest possible symmetry of the framework type, and they are based on model structures containing only silicon and oxygen. In contrast, the measured materials in this study contain germanium as well and were determined by a different method.

Table 3. Unit cell parameters of UTL. Comparison between Le Bail fitting of PXRD pattern, XDS program calculations, and theoretical values from the IZA database.

cell parameters	Le Bail	cRED	IZA
a [Å]	29.761(5)	30.240(120)	29.800
b [Å]	14.011(2)	14.312(6)	13.993
c [Å]	12.416(2)	12.569(14)	12.393
α [°]	90.000(0)	90.000(0)	90.000
β [°]	104.91(0)	105.318(170)	105.185
γ [°]	90.000(0)	90.000(0)	90.000

The program SHELXT was used to determine the structure of the parent material. A crystal structure solution was found in space group *C*2/m, in agreement with previously published reports. This obtained structure was then further refined by SHELXL in the OLEX2 program. The achieved R_1 factor was 23.91 %, which is acceptable for zeolite crystal structures determined through this method. The final, refined structure of the parent UTL material is shown in Figure 14.

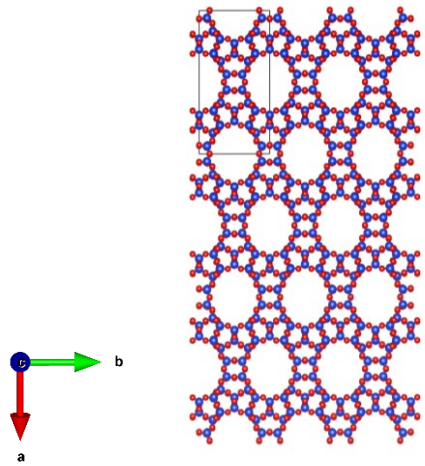

Figure 14. The refined structure of UTL, parent material.

VESTA software was utilized to analyze the pore sizes within the UTL material. UTL framework possesses 14-ring channels orientated along the c-axis, and 12-ring pore channels orientated along the b-axis. The diameters of these pores are 10.32 Å × 13.35 Å and 8.86 Å × 11.24 Å for 14-ring channel and 12-ring channel, respectively (Figure 15).

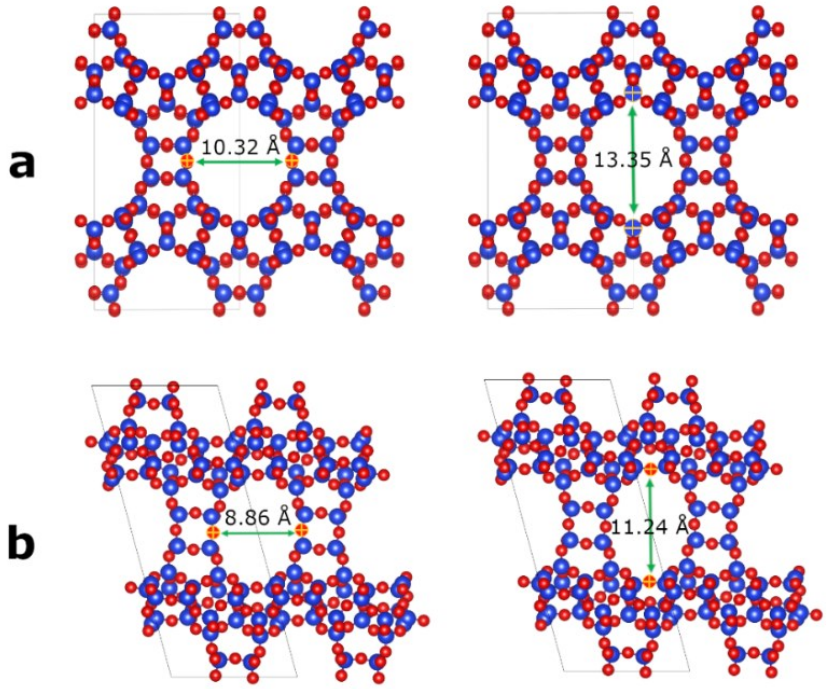

Figure 15. 14-ring channel (a) and 12-ring channel (b) of UTL and their sizes.

5.3 Structure determination of daughter materials

5.3.1 IPC-2

IPC-2 was the first investigated daughter material. The PXRD pattern was fitted by the Le Bail method. The parameters from IZA database were used as starting values. The resulting fit is shown in Figure 16. The obtained unit cell parameters with their deviations are presented in Table 4. The R_w value of the fit was 0.1023.

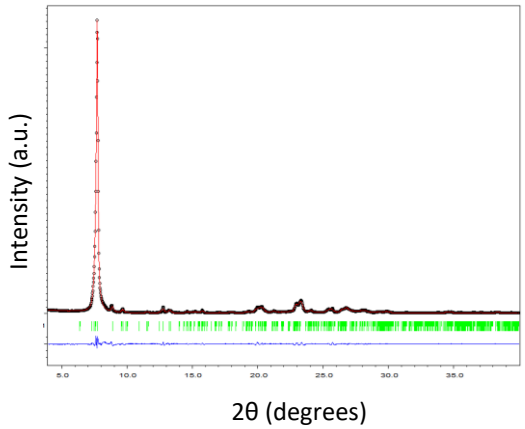

Figure 16. Le Bail fit of PXRD pattern of IPC-2.

cRED was utilized for structure determination of IPC-2. A total of 418 electron diffraction frames were collected across a range of −67.02 degrees to +46.64 degrees with a rotation speed of 0.681 degrees per second. The collected frames were then merged using the REDp program. Analysis of the merged data revealed a monoclinic C-centered Bravais lattice, and a 2/m Laue group, consistent with the parent material. The reflection conditions were determined by examining individual 2D plane slices. These conditions are identical to those observed for UTL, leading to the identification of three possible space groups for IPC-2: *C*2 (number 5), *C*m (number 8), or *C*2/m (number 12).

Subsequently, data reduction and integration were performed using the XDS program. The calculations confirmed a monoclinic C-centered (m*C*) Bravais lattice with these unit cell parameters: a = 24.644 Å, b = 13.924 Å, c = 12.429 Å, α = 90.000 °, β = 109.756 °, γ = 90.000 °. A detailed comparison of these values with their deviations and theoretical values is presented in Table 4. As previously mentioned, the discrepancies arise from the differences in measurement techniques and material composition. The data was integrated in the same way as the parent material. However, the resulting data exhibited a lower data completeness (71.6 %), but also a lower observed R factor (7.2 %).

Table 4. Unit cell parameters of IPC-2. Comparison between Le Bail fitting of PXRD pattern, XDS program calculations, and theoretical values from the IZA database.

cell parameters	Le Bail	cRED	IZA
a [Å]	24.360(9)	24.644(37)	24.132
b [Å]	13.964(5)	13.924(9)	13.792
c [Å]	12.419(5)	12.429(22)	12.298
α [°]	90.000(0)	90.000(0)	90.000
β [°]	109.128(0)	109.756(160)	109.600
γ [°]	90.000(0)	90.000(0)	90.000

The final structure of IPC-2 was determined using the SHELXT program. This process benefited significantly from prior knowledge of the parent material's structure, leading to a faster determination. The analysis confirmed the same space group (*C*2/m) as observed for the parent material.

Finally, the structure was further refined using the SHELXL in the OLEX2 program. This refinement process resulted in a lower R_1 factor (22.58 %) compared to the parent material. The final, refined structure of IPC-2 is shown in Figure 17.

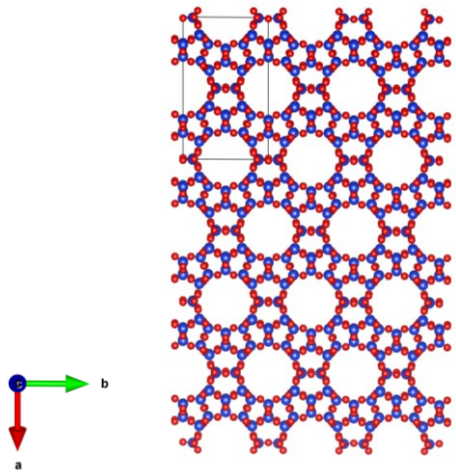

Figure 17. The refined structure of IPC-2.

IPC-2 framework contains 12-ring pore channels orientated along the c-axis, and 10-ring pore channels orientated along the b-axis. The VESTA program was utilized to analyze the pore's diameter. The pore diameter is 10.76 Å × 10.46 Å and 9.18 Å × 8.50 Å for 12-ring and 10-ring pores, respectively (Figure 18).

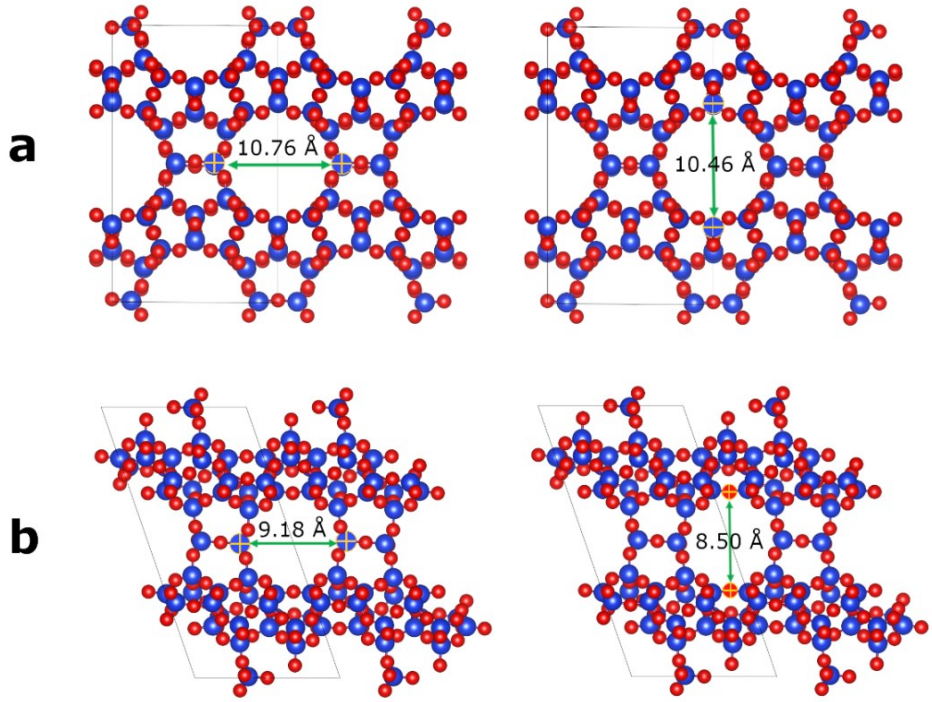

Figure 18. The size of 12-ring channel (a) and 10-ring channel (b).

5.3.2 IPC-4

IPC-4, the second daughter material of the UTL zeolite, was investigated using the same procedures as for the previous samples. The analysis began with fitting the PXRD pattern using the Le Bail method. The resulting fit is shown in Figure 19, and obtained unit cell parameters are presented in Table 5 with their deviations as well. The R_w value for this fit was 0.1876.

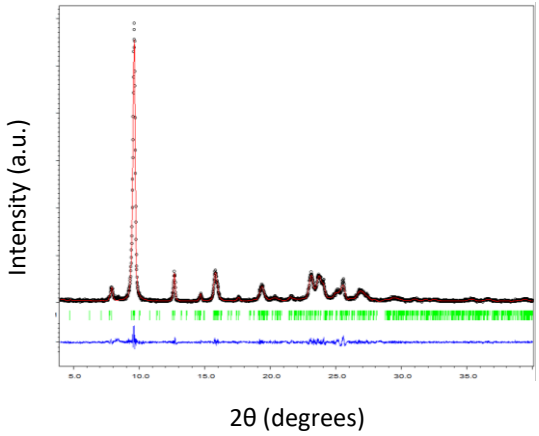

Figure 19. The Le Bail fit of IPC-4 PXRD pattern.

During the cRED, a total of 353 frames were collected across a rotation range of 96.87 degrees. The starting angle was −61,31 degrees, and the ending angle was +35.56 ° degrees, with a rotation speed of 0.688 degrees per second. The REDp program was used for initial investigation of the frames. Bravais lattice, Laue group, and space group determination was performed by analyzing the diffraction spots in 2D plane slices. The observed Bravais lattice (C-centered), Laue group (2/m) and the potential space groups were the same as in the case of the parent material.

Following the set workflow, the XDS program was used for reduction and integration to determine the unit cell parameters of IPC-4. The resulting monoclinic C-centered Bravais lattice had these unit cell parameters: a = 19.924 Å, b = 13.801 Å, c = 12.177 Å, α = 90.000 °, β = 114.477 °, γ = 90.000 °. A comparison of these values with theoretical values is presented in Table 5. As observed previously, there are minor discrepancies between the measured and theoretical values, which arise from the factors discussed earlier. The final data completeness was 69.5 %, with an observed R factor of 8.1 %.

Table 5. Unit cell parameters of IPC-4. Comparison between Le Bail fitting of PXRD pattern, XDS program calculations, and theoretical values from the IZA database.

cell parameters	Le Bail	cRED	IZA
a [Å]	18.210(10)	19.924(61)	20.114
b [Å]	13.611(7)	13.801(3)	13.956
c [Å]	12.115(5)	12.177(30)	12.351
α [°]	90.000(0)	90.000(0)	90.000
β [°]	114.656(0)	114.477(240)	114.800
γ [°]	90.000(0)	90.000(0)	90.000

The SHELXT program was utilized for structure determination of IPC-4. This process benefited from the previously established information about the parent material. Since IPC-4 shares the same morphology, Bravais lattice (C-centered), Laue group (2/m), and space group (*C*2/m) as the parent material, the structure determination was achieved more efficiently.

The final refinement of the IPC-4 structure was performed using SHELXL within the OLEX2 program. This refinement process resulted in the lowest R_1 factor (15.37 %) observed among all studied samples. As mentioned before, a lower R-factor signifies a better refined crystal structure model. The final, refined structure of IPC-4 is presented in Figure 20.

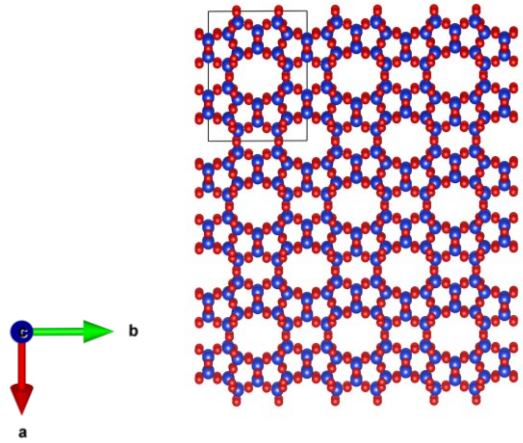

Figure 20. The refined structure of IPC-4.

Compared to UTL and IPC-2, IPC-4 contains the smallest pores. Its framework possesses of 10-ring channel and 8-ring channel pores. The 10-ring pores are orientated along the c-axis with diameter of 7.84 Å × 8.86 Å. The 8-ring channels are orientated along the b-axis and their diameter is 7.47 Å × 5.92 Å. These pore channels are shown in Figure 21.

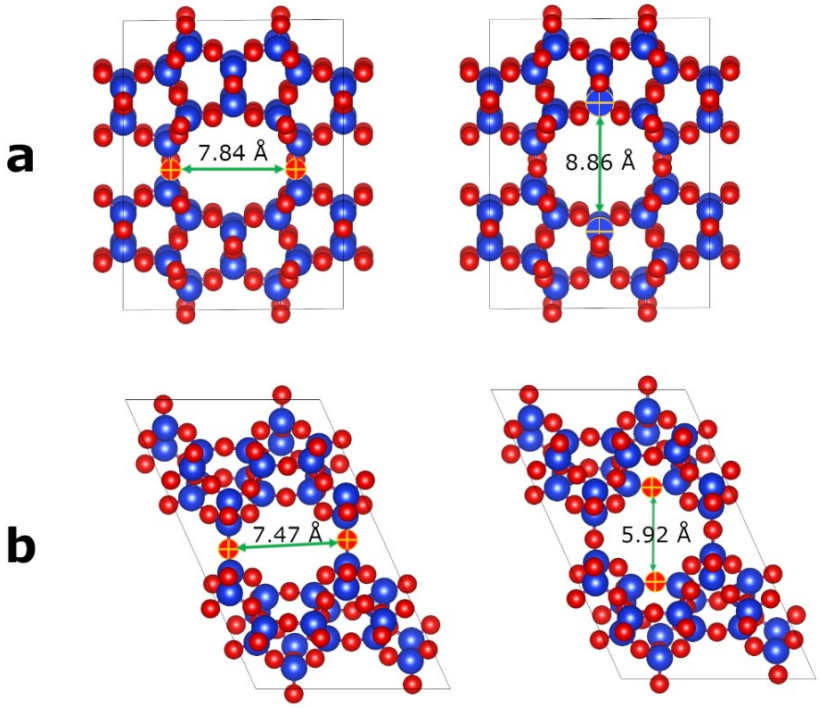

Figure 21. The size of 10-ring channel (a) and 8-ring channel (b).

5.4 Case study: IWV and daughter material IPC-20

To confirm the validity of established workflow a case study on another germanosilicate zeolite, i.e. IWV was performed. Recent discovery showed that IWV germanosilicate is a parent material for ADOR synthesis of IPC-20[77]. Samples of parent and daughter zeolites were provided by doc. Maksym Opanasenko, CSc.

Firstly, the samples were analyzed by common methods to gain knowledge about the crystallinity, morphology, and textural properties of these samples (Figure 22). PXRD patterns confirmed the crystallinity of both samples. Argon sorption analysis revealed the BET surface areas of 569 $m^2 \cdot g^{-1}$ and 379 $m^2 \cdot g^{-1}$ for IWV and IPC-20, respectively. Additionally, the total micropore volume was determined to be 0.22 $cm^3 \cdot g^{-1}$ for IWV and 0.14 $cm^3 \cdot g^{-1}$ for IPC-20. SEM images indicated a similar morphology for the crystals of both materials. Figure 22 presents structural similarities between parent (IWV) and daughter (IPC-20) materials. This observation shows, like in the case of UTL ADOR transformation discussed before, that the structural, textural and morphological properties of the parent material give us clear indication on how to investigate the structure of daughter zeolite.

PXRD patterns were fitted using Le Bail method. Obtained unit cell parameters with their deviations are presented in Table 6. The R_w factors for this fit were 0.1560 and 0.0617 for IWV and IPC-20, respectively.

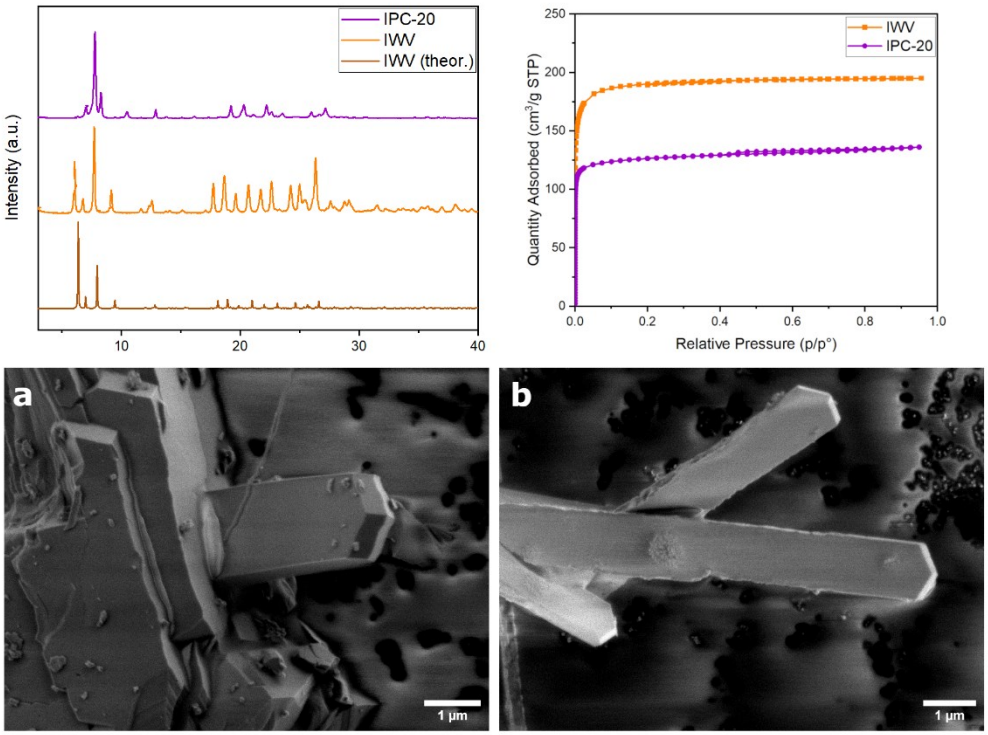

Figure 22. PXRD patterns and argon sorption isotherms for parent IWV (orange, brown for theoretical pattern) and daughter IPC-20 (violet). Morphology of IWV (a) and IPC-20 (b) is presented in SEM images.

The structure determination process began with a cRED measurement of parent IWV. During this measurement, 414 diffraction frames were collected across a rotation range of 111.84 degrees, starting from −54.41 degrees and ending at +57.43 degrees. Analysis of diffraction frames revealed a face-centered orthorhombic (o*F*) Bravais lattice and mmm Laue group. The calculated unit cell parameters are these: a = 13.684 Å, b = 25.209 Å, c = 28.305 Å, α = 90.000 °, β = 90.000 °, γ = 90.000 °. Table 6 provides a comparison of these obtained unit cell parameters with the values derived from Le Bail fitting and theoretical values retrieved from IZA database. The completeness of the diffraction data for the IWV material was 80.6 %, with an observed R factor of 18.5 %.

Table 6. Cell parameters of the IWV parent material derived from cRED measurement compared with the Le Bail fitting and theoretical ones from the IZA database.

cell parameters	Le Bail	cRED	IZA
a [Å]	14.538(1)	13.684(15)	13.944
b [Å]	25.864(3)	25.209(7)	26.081
c [Å]	27.523(3)	28.305(24)	27.826
α [°]	90.000(0)	90.000(0)	90.000
β [°]	90.000(0)	90.000(0)	90.000
γ [°]	90.000(0)	90.000(0)	90.000

The structure refinement revealed *F*mmm space group, and R_1 factor of 22.60 %. The resulting refined structure is shown in Figure 23.

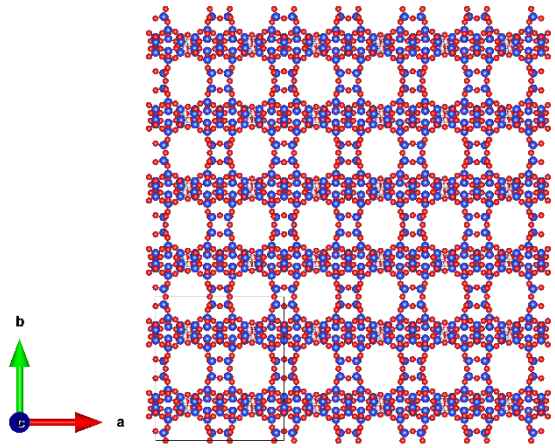

Figure 23. The refined structure of the IWV parent material.

Based on the similarities of crystal morphology and structural information about IWV parent material the determination of daughter IPC-20 was performed. During the cRED measurement, the 497 diffraction frames were collected, starting at –69.09 degrees and ending at +64.94 degrees. The analysis of diffraction frames revealed face-centered orthorhombic Bravais lattice (o*F*) as in the case of the parent material. The obtained cell parameters by XDS program are a = 13.575 Å, b = 22.303 Å, c = 24.914 Å, α = 90.000 °, β = 90.000 °, γ = 90.000 °. The unit cell parameters are presented in Table 7

compared with the values from Le Bail fitting and CCDC database[78] (CCDC number: 2203343). The data completeness for daughter material is 80.8 % with an observed R factor of 20.5 %.

Table 7. Cell parameters of IPC-20 daughter material derived from cRED compared with values from Le Bail fitting and CCDC database.

cell parameters	Le Bail	cRED	CCDC
a [Å]	13.777(1)	13.575(6)	13.8124(19)
b [Å]	22.772(1)	22.303(6)	22.711(6)
c [Å]	25.238(2)	24.914(7)	25.356(4)
α [°]	90.000(0)	90.000(0)	90.0(0)
β [°]	90.000(0)	90.000(0)	90.0(0)
γ [°]	90.000(0)	90.000(0)	90.0(0)

The space group of this material was determined as *F*mm2. The refined structure of IPC-20 had R_1 factor of 24.85 %. This daughter structure contains S4Rs instead of D4Rs, which is visible in Figure 24.

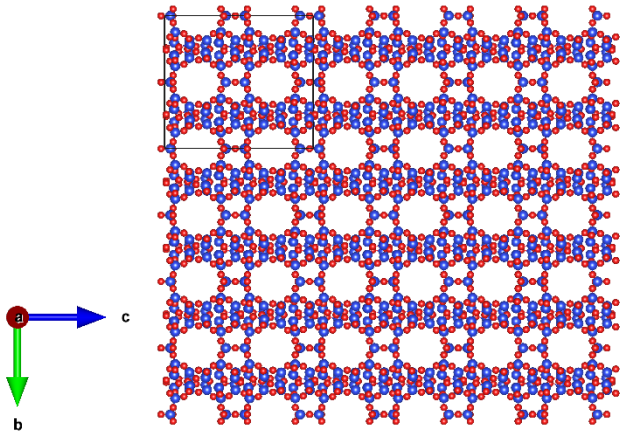

Figure 24. The refined structure of the IPC-20 daughter material.

The established workflow was proven to be suitable for fast structure determination of zeolites prepared by ADOR approach based on the information about a parent material. This shows that the workflow is universal and can provide structure solutions for diverse daughter materials.

6 Conclusions

This thesis successfully established a workflow for determining the structure of ADOR daughter zeolite materials by leveraging knowledge of the parent material (Figure 25). This approach involves detailed characterization of the parent material, consisting of morphology and texture analysis, investigation of the elemental composition, and structural determination including standard PXRD methods. After gaining a basic knowledge about the parent material, the advanced cRED technique is used for the structure solution. The information gained for the parent, well-known structure is then used for the analysis of potentially new daughter zeolites. This workflow was established on existing and approved pairs of the parent-daughter ADOR zeolites. The effectiveness of this approach was validated through a case study on a novel, recently discovered ADOR daughter material.

At first, the well-known parent UTL zeolite was synthesized. It was utilized for the synthesis of two different daughter materials, i.e., IPC-2 and IPC-4 using the ADOR approach. Parent and daughter materials underwent a series of standard characterization techniques, i.e. PXRD, SEM, STEM-EDS and argon sorption. The analyses revealed similarities between the parent and daughter materials, which significantly simplified subsequent structure determination by cRED.

The structure determination process began with a cRED measurement of the UTL parent material. Analysis of 2D slices extracted from the diffraction pattern facilitated the identification of potential space groups for the parent material. Subsequently, the program XDS was used for data reduction and integration, confirming the Bravais lattice as monoclinic C-centered (m*C*) and providing refined unit cell parameters. The structure of the parent UTL phase could be solved in the space group *C*2/m. This information was used as a starting point for the analysis of cRED data of IPC-2 and IPC-4 zeolites. Notably, both daughter materials shared the same Bravais lattice and space group as the parent material. The quality of the obtained crystal structures is reflected by the relatively low R_1 factors of the refined models. The final R values for the crystal

structures are 23.91%, 22.58%, and 15.37% for UTL, IPC-2, and IPC-4, respectively.

To demonstrate the wider applicability of this methodology to other ADORable zeolites, the workflow was successfully applied to parent material with another framework topology – IWV. The structure of a daughter material (IPC-20) derived from IWV germanosilicate was determined using cRED. Parent and daughter materials were first investigated by standard characterization methods giving the basic input for facile cRED measurements and data treatment. cRED analysis of IWV confirmed the assumed structure of this material. cRED data collection of IPC-20 was not trivial due to the presence of amorphous extra-phase in the provided sample. However, the insight gained during the analysis of parent material, mainly from SEM measurements, allowed to select the suitable crystal of the daughter zeolite. The structure of IPC-20 was determined subsequently, using the expertise obtained during solution of IWV. Both materials possess the same Bravais lattice (o*F*), however, different space groups. While space group *F*mmm was determined for the parent material, the crystal of IPC-20 was solved in space group *F*mm2. The calculated R_1 factors for these structures were again appreciably low with 22.60 % and 24.85 % for IWV and IPC-20, respectively. This case study showed the validity of the procedure and proved that it can be used for unknown ADOR daughter zeolites that would be synthesized in the future.

This work highlighted the effectiveness of utilizing the knowledge about the parent material gained by comprehensive structural studies to simplify the structure determination of derived daughter materials. Future research will focus on determination of the structures of other daughter materials with more complex pore systems derived from UTL, i.e. IPC-6 and IPC-7. Additionally, this method will be utilized for the investigation of daughter materials synthesized from other parent zeolites with various topologies. Some examples of ADORable germanosilicates that can produce novel zeolites are IWV, IWW, ITR, IWR, and ITH.[18] Further experiments will involve the application of rational ADOR approach with aim on synthesis of theoretically predicted but so far synthetically elusive, new zeolites. The workflow established in this thesis is an essential help

for the fast and facile verification of the success in preparation of ADOR zeolites, even at the early stages of the method optimization. It will allow to spot the new material even if the prepared samples are not free from the side-phases, such as remaining parent material or amorphous residues produced during the synthesis. In such cases, which are frequently observed during the early stages of novel ADOR zeolites syntheses optimization, the use of PXRD is inadequate for the structure determination, while cRED allows precise identification of the previously unknown structures.

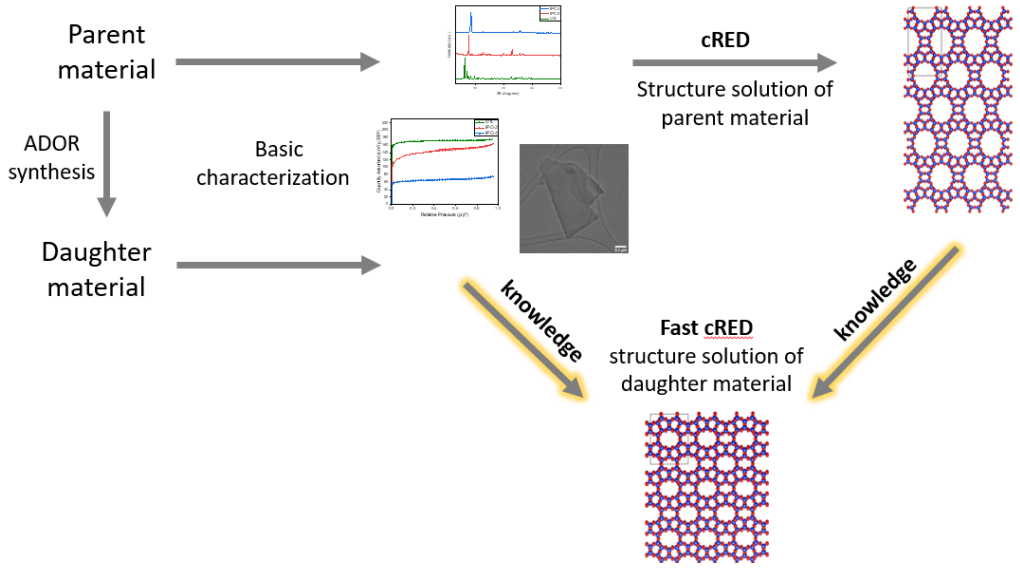

Figure 25. Scheme of the established procedure for the structure solution of daughter ADOR zeolite.

7 References

1. Primo, A.; Garcia, H.: Zeolites as catalysts in oil refining. *Chemical Society Reviews* **43**, 7548–7561 (2014).

2. Davis, M. E.: Zeolites from a Materials Chemistry Perspective. *Chemistry of Materials* **26**, 239–245 (2014).

3. Mazur, M. *et al.*: Germanosilicate UTL and its rich chemistry of solid-state transformations towards IPC-2 (OKO) zeolite. *Catalysis Today* **243**, 23–31 (2015).

4. Weitkamp, J.: Zeolites and catalysis. *Solid State Ionics* **131**, 175–188 (2000).

5. Čejka, J. *et al.*: Zeolite-based materials for novel catalytic applications: Opportunities, perspectives and open problems. *Catalysis Today* **179**, 2–15 (2012).

6. Eliášová, P. *et al.*: The ADOR mechanism for the synthesis of new zeolites. *Chemical Society Reviews* **44**, 7177–7206 (2015).

7. Zhang, J. *et al.*: Toward Controlling Disassembly Step within the ADOR Process for the Synthesis of Zeolites. *Chemistry of Materials* **33**, 1228–1237 (2021).

8. Paillaud, J. L. *et al.*: Extra-Large-Pore Zeolites with Two-Dimensional Channels Formed by 14 and 12 Rings. *Science* **304**, 990–992 (2004).

9. Shvets, O. V. *et al.*: UTL zeolite and the way beyond. *Microporous and Mesoporous Materials* **182**, 229–238 (2013).

10. Roth, W. J. *et al.*: A family of zeolites with controlled pore size prepared using a top-down method. *Nature Chemistry* **5**, 628–633 (2013).

11. Přech, J. *et al.*: From 3D to 2D zeolite catalytic materials. *Chemical Society Reviews* **47**, 8263–8306 (2018).

12. Passaglia, E.; Sheppard, R. A.: The Crystal Chemistry of Zeolites. *Reviews in Mineralogy and Geochemistry* **45**, 68–116 (2001).

13. Database of zeolite structures. http://www.iza-structure.org/databases/ (accessed 15.1.2024)

14. Veselý, O.; Morris, R. E.; Čejka, J.: Beyond traditional synthesis of zeolites: The impact of germanosilicate chemistry in the search for new materials. *Microporous and Mesoporous Materials* **358**, (2023).

15. Serati-Nouri, H. *et al.*: Biomedical applications of zeolite-based materials: A review. *Materials Science and Engineering C* **116**, 111225 (2020).

16. Chen, L. H. *et al.*: Hierarchically Structured Zeolites: From Design to Application. *Chemical Reviews* **120**, 11194–11294 (2020).

17. Mazur, M. *et al.*: Synthesis of 'unfeasible' zeolites. *Nature Chemistry* **8**, 58–62 (2016).

18. Trachta, M.; Nachtigall, P.; Bludský, O.: The ADOR synthesis of new zeolites: In silico investigation. *Catalysis Today* **243**, 32–38 (2015).

19. van Bokhoven, J. A.; Lamberti, C.: Structure of aluminum, iron, and other heteroatoms in zeolites by X-ray absorption spectroscopy. *Coordination Chemistry Reviews* **277**, 275–290 (2014).

20. Opanasenko, M. *et al.*: Synthesis and Post-Synthesis Transformation of Germanosilicate Zeolites. *Angewandte Chemie International Edition* **59**, 19380–19389 (2020).

21. Shamzhy, M. V. *et al.*: Post-Synthesis Stabilization of Germanosilicate Zeolites ITH, IWW, and UTL by Substitution of Ge for Al. *Chemistry - A European Journal* **22**, 17377–17386 (2016).

22. Li, J.; Corma, A.; Yu, J.: Synthesis of new zeolite structures. *Chemical Society Reviews* **44**, 7112–7127 (2015).

23. Derbe, T.; Temesgen, S.; Bitew, M.: A Short Review on Synthesis, Characterization, and Applications of Zeolites. *Advances in Materials Science and Engineering* **2021**, (2021).

24. Čejka, J.; van Bekkum, H.; Corma, A.: *Introduction to Zeolite Molecular Sieves*. 3rd edition, Elsevier, 2007.

25. Wheatley, P. S. *et al*.: Novel zeolites with Continuously Tuneable Porosity. *Angewandte Chemie* **126**, 13426–12430 (2014).

26. Siegrist, T.: *X-Ray Structure Analysis.* Berlin, Boston, De Gruyter, 2022.

27. Li, J.; Sun, J.: Application of X-ray Diffraction and Electron Crystallography for Solving Complex Structure Problems. *Accounts of Chemical Research* **50**, 2737–2745 (2017).

28. Erich H. K.; Howard Ch. J.: *Applications of Neutron Powder Diffraction*. Oxford University Press, 2012.

29. Finney, J. L.: The Complementary Use of X-ray and Neutron Diffraction in the Study of Crystals. *Acta Crystallographica Section B* **51**, 447–467 (1995).

30. Ermrich, M.; Opper, D.: *XRD for the Analyst*. Revised edition, Almelo, Malvern Panalytical B.V., 2018.

31. Ameh, E. S.: A review of basic crystallography and x-ray diffraction applications. *International Journal of Advanced Manufacturing Technology* **105**, 3289–3302 (2019).

32. Huang, Z.; Willhammar, T.; Zou, X.: Three-dimensional electron diffraction for porous crystalline materials: structural determination and beyond. *Chemical Science* **12**, 1206–1219 (2021).

33. Shih, K.: *X-Ray Diffraction Structure, Principles and Applications*. New York, Nova Publishers, 2013.

34. Harris, K. D. M.; Tremayne, M.; Kariuki, B. M.: Contemporary Advances in the Use of Powder X-ray Diffraction for Structure Determination. *Angewandte Chemie - International Edition* **40**, 1626–1651 (2001).

35. Holder, C. F.; Schaak, R. E.: Tutorial on Powder X-ray Diffraction for Characterizing Nanoscale Materials. *ACS Nano* **13**, 7359–7365 (2019).

36. Dorset, D. L.; Roth, W. J.; Gilmore, C. J.: Electron crystallography of zeolites - the MWW family as a test of direct 3D structure determination. *Acta Crystallographica A* **61**, 516–527 (2005).

37. Li, J. *et al.*: Structure Solution and Defect Analysis of an Extra-Large Pore Zeolite with UTL Topology by Electron Microscopy. *Journal of Physical Chemistry Letters* **11**, (2020).

38. Dong, Z.: *Fundamentals of Crystallography, Powder X-Ray Diffraction, and Transmission Electron Microscopy for Materials Scientists*. CRC Press, Taylor & Francis Group, 2022.

39. Willhammar, T.; Yun, Y.; Zou, X.: Structural Determination of Ordered Porous Solids by Electron Crystallography. *Advanced Functional Materials* **24**, 182–199 (2014).

40. Su, J. *et al.*: Structure analysis of zeolites by rotation electron diffraction (RED). *Microporous and Mesoporous Materials* **189**, 115–125 (2014).

41. Luo, Y. *et al.*: Atomic-scale insights into topotactic transformations in extra-large pore silicate zeolites using time-resolved 3D electron diffraction. *ChemRxiv* (2024). DOI: 10.26434/chemrxiv-2023-pdtg4-v2

42. Li, Y.; Ling, Y.; Ma, Y.: Application of three-dimensional electron diffraction in structure determination of zeolites. *Chinese Journal of Structural Chemistry*, 100237 (2024).

43. Gruene, T.; Mugnaioli, E.: 3D Electron Diffraction for Chemical Analysis: Instrumentation Developments and Innovative Applications. *Chemical Reviews* **121**, 11823–11834 (2021).

44. Wan, W. *et al.*: Transmission electron microscopy as an important tool for characterization of zeolite structures. *Inorganic Chemistry Frontiers* **5**, 2836–2855 (2018).

45. Gemmi, M.; Lanza, A. E.: 3D electron diffraction techniques: The Nanocrystallography Revolution. *ACS Central Science* **5**, 1315-1329 (2019).

46. Cichocka, M. O. *et al.*: High-throughput continuous rotation electron diffraction data acquisition via software automation. *Journal of Applied Crystallography* **51**, 1652–1661 (2018).

47. Inkson, B. J.: *Scanning Electron Microscopy (SEM) and Transmission Electron Microscopy (TEM) for Materials Characterization*. Elsevier Ltd, 2016.

48. Cazaux, J.: From the physics of secondary electron emission to image contrasts in scanning electron microscopy. *Journal of Electron Microscopy* **61**:5, 261–284 (2012).

49. Kannan, Dr. M.: Scanning Electron Microscopy: Principle, Components and Applications. *Textbook on Fundamentals and Applications of Nanotechnology,* 82–92 (2018).

50. Luo, Z. *A: Practical Guide to Transmission Electron Microscopy: Fundamentals*. New York, Momentum Press, 2016.

51. Zuo, J. M.; Spence, J. C. H.: *Advanced Transmission Electron Microscopy: Imaging and Diffraction in Nanoscience.* New York, Springer, 2016.

52. Sardela, M.: *Practical Materials Characterization*. New York, Springer, 2014.

53. Tang, C. Y.; Yang, Z.: *Transmission Electron Microscopy (TEM)*. *Membrane Characterization*. Elsevier, 2017.

54. Hodoroaba, V. D.: *Energy-Dispersive X-Ray Spectroscopy (EDS)*. *Characterization of Nanoparticles: Measurement Processes for Nanoparticles.* Elsevier, 2019

55. Mishra, R. K.; Thomas, S.; Zachariah, A. K.: *Energy-Dispersive X-Ray Spectroscopy Techniques for Nanomaterial*. *Microscopy Methods in Nanomaterials Characterization.* Elsevier, 2017.

56. Thommes, M.: *Physical Adsorption Characterization of Ordered and Amorphous Mesoporous Materials*. *Nanoporous Materials: Science and Engineering.* Imperial College Press, 2004.

57. Xu, R.; Prodanović, M.: Effect of pore geometry on nitrogen sorption isotherms interpretation: A pore network modeling study. *Fuel* **225**, 243–255 (2018).

58. Ruthven, D. M.: Characterization of zeolites by sorption capacity measurements. *Microporous and Mesoporous Materials* **22**, 537–541 (1998).

59. Pérez-Botella, E.; Valencia, S.; Rey, F.: Zeolites in Adsorption Processes: State of the Art and Future Prospects. *Chemical Reviews* **122**, 17647–17695 (2022).

60. Seibel, Ch. *et al.*: Sorption measurements for determining surface effects and structure of solid fuels. *Fuel Processing Technology* **153**, 81–86 (2016).

61. Mel'gunov, M. S.: Application of the simple Bayesian classifier for the N2 (77 K) adsorption/desorption hysteresis loop recognition. *Adsorption* **29**, 199–208 (2023).

62. Rahman, M. M. *et al*: A Statistical Approach to Determine Optimal Models for IUPAC-Classified Adsorption Isotherms. *Energies* **12**, 4565 (2019).

63. Chang, Q.: *Surface of Solids*. *Colloid and Interface Chemistry for Water Quality Control.* Elsevier, 2016.

64. Marino, M. G.; Kreuer, K. D.: Alkaline stability of quaternary ammonium cations for alkaline fuel cell membranes and ionic liquids. *ChemSusChem* **8**, 513–523 (2015).

65. Čejka, J. *et al.*: The role of template structure and synergism between inorganic and organic structure directing agents in the synthesis of UTL zeolite. *Chemistry of Materials* **22**, 3482–3495 (2010).

66. Petříček, V. *et al.*: Jana 2020 - a new version of the crystallographic computing system Jana. *Zeitschrift für Kristallographie–Crystalline Materials* **238**, 271–282 (2023).

67. Smeets, S. *et al.*: Instamatic. *Instamatic (1.0.0)* https://doi.org/10.5281/zenodo.2026774 (2018).

68. Wan, W. *et al.*: Three-dimensional rotation electron diffraction: Software RED for automated data collection and data processing. *Journal of Applied Crystallography* **46**, 1863–1873 (2013).

69. Kabsch, W.: XDS. *Acta Crystallographica D Biological Crystallography* **66**, 125–132 (2010).

70. Sheldrick, G. M.: A short history of SHELX. *Acta Crystallographica A* **64**, 112–122 (2008).

71. Sheldrick, G. M.: SHELXT - Integrated space-group and crystal-structure determination. *Acta Crystallographica A* **71**, 3–8 (2015).

72. Ge, M. *et al.*: On the Completeness of Three-Dimensional Electron Diffraction Data for Structural Analysis of Metal-Organic Frameworks. *Faraday Discussions* **231**, 66–80 (2021).

73. McRee, D. E.: *Practical Protein Crystallography*. San Diego, Academic Press, 1999.

74. Online Dictionary of Crystallography. https://dictionary.iucr.org/R_factor. (accessed 10.5.2024)

75. Shmueli, U.; Flack, H. D.; Spence, J. C. H.: Methods of space-group determination. *International Tables for Crystallography,* 107–131 (2016).

76. Baerlocher, Ch.; Hepp, A.; Meier, W. M.: *DLS-76, a program for the simulation of crystal structures by geometric refinement.* Zuerich, Institute of Crystallography and Petrography, 1977.

77. Yue, Q. *et al.*: Catching a New Zeolite as a Transition Material during Deconstruction. *Journal of the American Chemical Society* **145**, 9081–9091 (2023).

78. The Cambridge Crystallographic Data Centre. https://www.ccdc.cam.ac.uk/. (accessed 23.4.2024)